Multiplicities and angular distributions in deep-inelastic *ep* and *en* scattering*

B. Gibbard, K. Berkelman,† P. H. Garbincius,‡ J. S. Klinger, and P. Wanderer§
Laboratory of Nuclear Studies, Cornell University, Ithaca, New York 14850

A. J. Sadoff
Physics Department, Ithaca College, Ithaca, New York 14850

(Received 15 May 1974)

We report charged hadron multiplicities and inclusive angular distributions in deep-inelastic electron-proton and electron-neutron scattering in the kinematic range $1.4 \leq Q^2 \leq 8$ GeV^2 and $3 \leq s \leq 14$ GeV^2. At the lowest s values we observe that the *ep* mean multiplicity is somewhat less than in photoproduction. This is associated with a relative increase in one-prong events and a decrease in three-prong events. Also at low s the *en* multiplicity is lower than the *ep* multiplicity. At higher s values the *ep* and *en* multiplicities are essentially equal and independent of Q^2 at fixed s. The relative topological cross sections, the pseudorapidity distributions, and the azimuthal angle dependence are also independent of Q^2.

I. INTRODUCTION

Much of the recent interest in hadron collisions at high energy has focused on global features of the final states, such as the dependence of the average charged hadron multiplicity on the squared center-of-mass energy s, the relative yields in the various multiplicities, and the single-particle inclusive distributions in longitudinal and transverse momentum. One can use the experimental data to test a number of hypotheses—limiting fragmentation, Feynman scaling, and short-range order in rapidity, for example—as well as to make detailed comparisons with statistical, multiperipheral, resonance, Regge, parton, and other models.[1]

We can expect the same kind of global information to be even more interesting for the hadron final states in deep-inelastic electron scattering. The final-state multiplicities and inclusive spectra in the virtual-photon–nucleon collision can vary with the virtual photon mass squared, $q^2 = -Q^2 < 0$, as well as with s, and in many models the Q^2 dependence is a unique probe of the short-distance internal structure of the nucleon. Although the theories which are still surviving tend to have rather similar predictions for hadron collisions, their predictions for electroproduction final states can be quite different. To see an example of this, suppose we consider the range of predictions for the Q^2 dependence of $\bar{n}$, the mean charged multiplicity.

A. Thermodynamic models

In any picture in which some kind of equilibrium is established before the final state evolves, one expects the multiplicity to depend only on the total center-of-mass energy, or perhaps entropy.[2] That is, $\bar{n}(s, Q^2)$ should be independent of Q^2 at fixed s. Or starting from the hypothesis of short-range order in rapidity,[1] the fact that the distribution of final-state hadrons in rapidity has the form of a plateau, the height of which is independent of projectile, target, or the value of s, implies that the mean multiplicity, which is the integral of the plateau divided by the cross section, is just a constant times the rapidity range, which is $\ln s$.

B. Photon fragmentation models

A spacelike photon is not an ordinary projectile. It cannot exchange a little momentum with the target and then fragment. In order to produce final-state particles on the mass shell, the virtual photon must in effect pick up a fraction $x = Q^2/2M\nu$ of the target nucleon, "pulverize" it, and throw it forward.[3] These pulverization fragments (or parton fragments if you prefer), having undergone a considerable change in momentum, might be expected to show up as a high multiplicity jet, the mean multiplicity increasing with x. One suggestion[3] is that $\bar{n} = K\nu^{\alpha(x)}$, where $\alpha(x)$ is an increasing function of x. The argument can be phrased in terms of the rapidity distribution.[4] The photon fragmentation region is not just a rapidity range of about two units at the forward end of the rapidity scale as it would be for an ordinary projectile, but instead shows up as a plateau of width $\ln Q^2$. This photon plateau may very well have a height C_p greater than the height C_c of the remaining plateau, and thus $\bar{n}(s, Q^2) = C_c \ln s + (C_p - C_c) \ln Q^2$, increasing with Q^2 at fixed s. Some versions of the parton model[4,5] share this feature.

C. Scaling models

If $\bar{n}(s, Q^2)$ were a function only of s/Q^2, then since $\bar{n}$ must increase with s at fixed Q^2, it would have to decrease with Q^2 at fixed s. The soft-field-theory parton model[6] and the multiperipheral model[7] suggest $\bar{n} = C\ln\omega$.

Thus, depending on one's theoretical prejudice, $\bar{n}(s, Q^2)$ will increase, decrease, or remain the same, as Q^2 is increased at fixed s.

Until now measurements of the charged hadron multiplicity in electroproduction have been performed using a volume track chamber, either a streamer chamber containing a liquid hydrogen target[8] or a liquid hydrogen bubble chamber.[9] In either case, the fact that one can tolerate only a limited number of beam particles per picture imposes a severe limitation on the usable incident beam intensity, implying a lower limit on the measurable cross section, and hence an upper limit on Q^2. To remove this restriction we have made the hadron-electron coincidence resolving time as short as possible by using scintillation counters to detect the hadrons. This enabled us to use an average incident beam intensity as high as 10^9 per second. The longer beam duty cycle of a synchrotron, as compared to a linac, was crucial too, of course.

With a finite number of scintillators (68) to cover essentially all of the solid angle around the target, we had to sacrifice detailed angular resolution and any hope of measuring momenta. However, for multiplicities and the gross features of the single-particle rapidity spectrum, such measurements are fortunately not necessary. We are then able to reach Q^2 values up to 8 GeV^2, much higher than in any previous coincidence electroproduction experiment, and we can explore the region of large x where the structure functions are varying significantly.[10]

II. BEAM AND TARGET

Figure 1 shows the layout of the experiment. The extracted electron beam of the Cornell synchrotron passed through a 2.6-cm liquid hydrogen target and on to a secondary emission beam monitor. At 92 cm downstream of the target the beam passed through the gap of the spectrometer magnet inside a heavy iron shield pipe located in the reduced field region between the magnet coils. At the target the beam spot was typically 3 mm in diameter, with an angular divergence of about 0.3 mrad.

The beam pulse rate was 60 per second, each pulse having up to 1.5×10^7 electrons and lasting for about 1.6 msec. During the beam pulse the intensity had a 2.5-μsec time structure corresponding to the circulation period in the synchrotron ring, which resulted in a typical duty cycle of about 50% during the beam pulse. The over-all beam duty cycle was therefore about 4%.

During the course of the experiment, data runs were taken with 7.0- and 11.5-GeV synchrotron energies. Because the instantaneous beam energy varied sinusoidally, there was a spread in energies of about 2% during the extraction time. This did not affect the accuracy of the data, since the instantaneous beam energy was recorded with the data for each event observed. This beam energy measurement has been calibrated by magnet deflection[11] to an accuracy of 0.3%.

III. ELECTRON DETECTION

Scattered electrons were detected in a spectrometer consisting of a 30D40 bending magnet

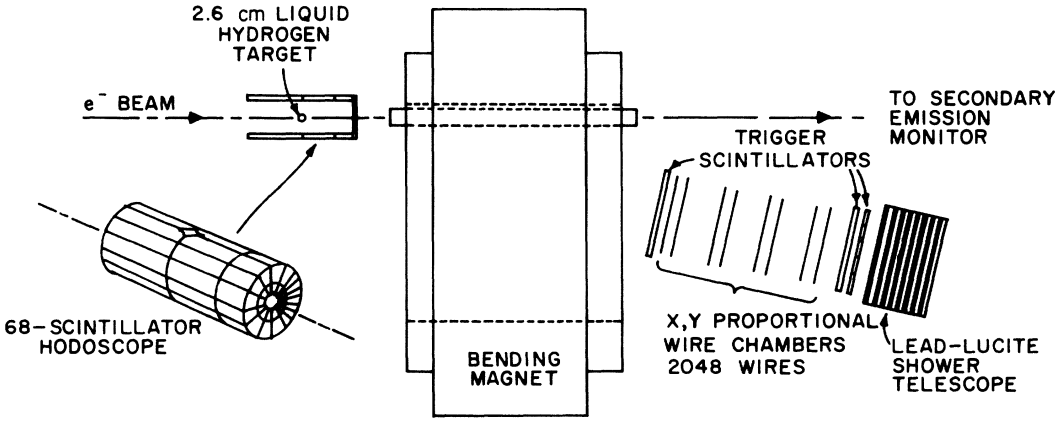

FIG. 1. Layout of the experiment.

(40 cm gap, 12 kG field), eight 50×50 cm^2 proportional wire planes,[12] three planes of scintillation counters, and a lead-Lucite shower telescope.[13] The aperture covered a solid angle of about 30 msr for all momenta greater than about 1 GeV/c, and extended from 9° to 20° in the "near geometry" data runs, and from 14° to 25° in the "far geometry" runs with the detectors moved farther from the beam line. Of the eight chamber planes, four had vertical wires and four horizontal. The track finding efficiency, judging from the observed number of tracks in which one of the four planes did not fire, was always greater than 99.5%. Multiple track events were rare and were usually resolved by noting which counters fired in the second and third planes of scintillators, which were divided into five and six intervals in the horizontal and vertical, respectively.

We extended the horizontal projection of each track back through the magnet gap, varying the radius of curvature until the extrapolated track intersected the center of the target. The momentum was then calculated from the radius of curvature and the known magnetic field. The track was rejected if the vertical projection, extended back through the magnet to the target, missed the beam height by more than 3 cm. The root-mean-square momentum resolution was approximately $\Delta p/p = p/(110\ \text{GeV}/c)$; the angular resolution was about 2 mrad. Resolution was limited by wire spacing, target size, multiple scattering, and radiation—all of comparable importance.

Electrons were distinguished from other negative particles (mainly π^-) by requiring a large pulse in the shower detector—eight 2.5-cm thick lucite Čerenkov counters interleaved with 1.1-radiation-length sheets of lead. In the analysis we required that each event satisfy each of the following criteria:

(1) The combined shower counter pulse height must exceed the 2.1 GeV level (the trigger threshold was about 1 GeV);

(2) The ratio of the shower pulse height (plus 2.8 GeV) and the reconstructed momentum must be greater than 0.88;

(3) The shower development must start in the first 2.2 radiation lengths of the detector;

(4) The calculated s value for the scattering must be less than 16 GeV^2. The latter criterion eliminated the low momentum end of the electron spectrum, where the pion contamination was largest and most difficult to resolve using pulse heights.

These four cuts not only eliminated practically all of the pion background; they also caused a loss of electron events, especially at the higher s values. For this reason it was not possible to make accurate comparisons of the observed electron scattering rates with predictions based on the known cross sections. Fortunately, however, we do not need to observe all scattering events to study the hadron final-state multiplicities and angular distributions; we require only that those events which are accepted at each Q^2 and s form an unbiased sample. Figure 2 shows the spectrum of shower pulse height, divided by momentum, before and after applying cuts (1) and (2), cuts (3) and (4) already having been applied.

In the 11.5 GeV near-geometry hydrogen data 28% of the triggers had no track (most of these were caused by photons or random coincidences), 38% were rejected because the track was made by a positively charged particle (positive particles produced at small angles were deflected by the magnet into the same region of the detector as the larger angle electrons), 0.7% were rejected in the vertical reconstruction cut, 13% were eliminated by the various shower counter cuts, and 20% were accepted in the analysis. Similar results were obtained for the other runs.

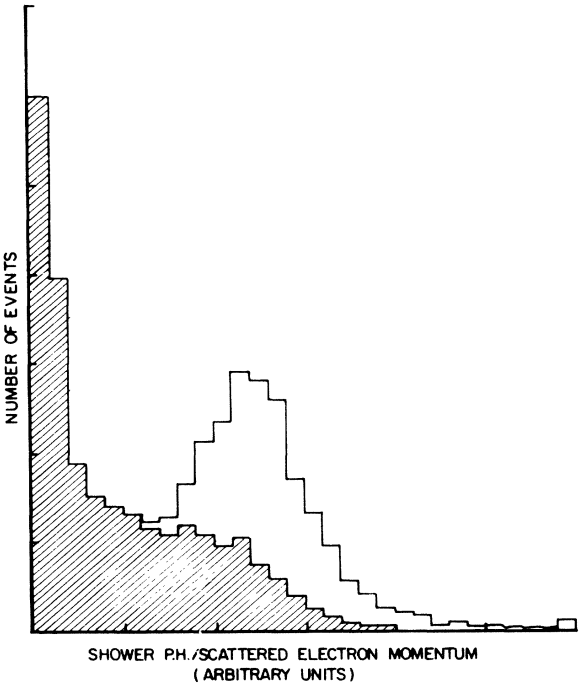

FIG. 2. Sample spectrum of pulse height in the shower telescope (the eight layers summed), divided by reconstructed momentum. Events not satisfying criteria (3) and (4) (see text) have already been eliminated. The shaded portion indicates the events rejected by cuts (1) and (2); the unshaded events are accepted as electrons.

IV. HADRON DETECTION

A single layer of 68 6-mm-thick scintillation counters completely enclosed the target, except for the 3° forward cone, the 20° backward cone, and a small hole above the target to accommodate the liquid hydrogen refrigerator line. The counters were arranged along the side and end of a cylinder (see Fig. 1) of 25 cm diameter with axis along the beam line. Two rings of scintillators covering the angular ranges 3° to 10° and 10° to 20° formed the end face 36 cm downstream of the target. Three more rings covering the angular ranges 20° to 30°, 30° to 90°, and 90° to 160° formed the cylindrical side. Each of the five rings was subdivided into 12 equal azimuthal segments. In the first two rings the four segments on the side of the beam opposite the electron spectrometer were further subdivided in two in order to improve the angular resolution near the virtual-photon direction. Using a radioactive source, we set the photomultiplier[14] high voltages for the 68 counters so that each would count minimum-ionizing particles with at least 99% efficiency. This calibration was repeated often throughout the course of the experiment.

Between the target and scintillators was the 1.3-mm-thick aluminum vacuum pipe. Extra material (polyethylene) was added in the large-angle range to equalize somewhat the material through which particles produced at various angles had to pass in order to reach the counters. The thickness, including target, pipe, and extra absorber, varied from 1.3 g/cm^2 to 2.3 g/cm^2. For protons this implied a minimum detectable momentum of typically 260 MeV/c, for pions about 70 MeV/c.

The event trigger consisted of a fast (~10 nsec) coincidence in the electron spectrometer between the first scintillator, at least one counter in each of the second and third scintillator planes, the shower telescope (mixed output of the eight Lucite Čerenkov counters), and any one of the six hadron scintillators which spanned the aperture of the electron spectrometer. Note that only an electron signal was required in the event trigger. No event selection was made on the basis of hadron information. For each event trigger we recorded the total pulse height in the shower telescope, the summed pulse height of the first two shower counters, the information from the proportional chamber wires, a "zero" or "one" bit ("latch") for each hadron scintillator depending on whether it fired within the 6.5 nsec coincidence gate, and the pulse height and time (relative to the electron trigger) of each hadron scintillator pulse. Also recorded were the instantaneous synchrotron energy and the spectrometer magnet current. The hadron counter pulse height and timing data were continually checked to monitor the efficiencies during the course of the experiment. Only the latch data, however, were used in the analysis of multiplicities and angular distributions.

The most serious background in the experiment came from random coincidences in the hadron detector array. In order to get an accurate sample of accidental hadron scintillator pulses without wasting beam time, we provided a concurrent "fake" event trigger in addition to the "real" event trigger just described. Since it is important that the fake trigger rate be proportional to the instantaneous beam intensity, it was obtained from a two-counter scintillator telescope aimed at a thin foil vacuum window in the beam line downstream of the spectrometer. We verified that the fake events were uncorrelated with the real events, and that the accidental hadron coincidence probabilities were the same as measured with a delayed real event trigger. Each fake trigger caused the same information to be recorded as in the case of real triggers, except that an extra bit was set to tag the fake event for the analysis. The fake event trigger rate was adjusted to be higher than the real rate, so that the statistical accuracy of the measured accidental probability for each scintillator was an order of magnitude better than for the real data.

V. DATA TAKING

For each accepted electron scattering event we use the instantaneous synchrotron energy E and the reconstructed electron scattered energy E' and angles θ_e and ϕ_e to calculate the square of the four-momentum transfer

$$Q^2 = 2EE'(1-\cos\theta_e), \tag{1}$$

the square of the final-state hadron total center-of-mass energy

$$s = 2M(E-E') + M^2 - Q^2, \tag{2}$$

and the direction of the virtual photon lab momentum

$$\tan\theta_\gamma = E'\sin\theta_e/(E-E'\cos\theta_e), \tag{3}$$

$$\phi_\gamma = \phi_e + \pi. \tag{4}$$

The momentum and angle resolution of the electron spectrometer imply 0.5 GeV^2 resolution (rms) in Q^2 and 2 GeV^2 in s. This is not high resolution according to the standards set by previous single-arm scattering experiments or exclusive electroproduction experiments, but it is quite adequate for studying the Q^2 and s dependences of hadron multiplicities and other slowly

varying features of the final states.

In order to cover a wider range of Q^2 and s than could be covered in one setting of our experimental conditions, we made three different runs (with both hydrogen and deuterium targets): $E = 7.0$ GeV near-geometry, $E = 11.5$ GeV near-geometry, and 11.5 GeV far-geometry. Table I summarizes the conditions for the three runs. The distribution of events in Q^2 and s for the hydrogen data is shown in Fig. 3. It is possible to identify in this figure the three slightly overlapping bands of data. For the multiplicity analysis the data were organized into 36 bins (some of them empty, actually) defined by six intervals in Q^2 and six intervals in s. Since there are not enough data to make a longitudinal–transverse separation measurement, we have ignored the possible dependence of the data on the virtual-photon polarization parameter ϵ. It varied from $\epsilon \approx 0.9$ at the lowest Q^2 and s to $\epsilon \approx 0.4$ at the highest Q^2 and s. The spread in ϵ for any single Q^2, s bin was typically less than 0.1.

The incident beam intensity was fixed by balancing our desire for statistical accuracy up to the highest Q^2 obtainable against the deterioration in data quality caused by a large random coincidence subtraction. As our confidence in the accidental correction, based on the fake trigger data, increased during the course of the experiment, we gradually increased the beam intensity until about 25% of all hadron counts were accidentals. This occurred at a beam intensity of about 1.5×10^7 electrons per pulse (60 pulses per second), which, although it is less than 0.1% of what the synchrotron can deliver, is still many times larger than used in previous electroproduction multiplicity experiments.[8,9] The maximum instantaneous singles counting rate in a hadron scintillator was 3×10^6 per second. A typical electron trigger rate was one per second.

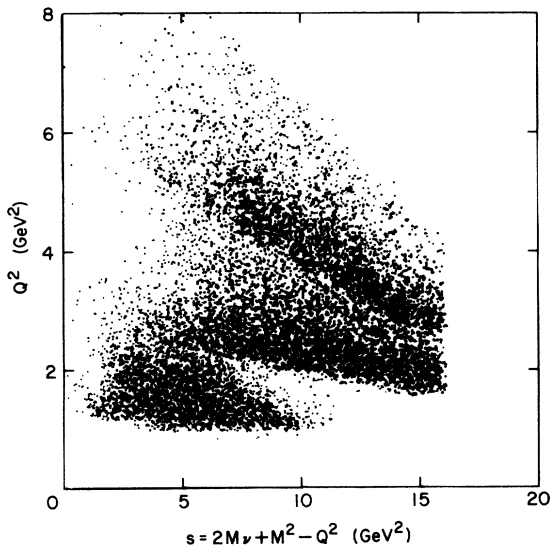

FIG. 3. Distribution of events in Q^2 and s for part of the hydrogen-target data.

In addition to the normal data runs, further runs were taken with empty target, with delayed coincidences, and with various absorbing materials between target and scintillators in order to check backgrounds. The 0.013-mm Kapton target wall was responsible for 5% of the observed electron rate and produced a mean charged multiplicity only slightly higher than did the hydrogen or deuterium. This was easily corrected using the empty-target data.

VI. MULTIPLICITY ANALYSIS: PROTON TARGET

A. Radiative correction

The electron can lose energy by radiation either in the deep-inelastic process itself or in the material through which the electron must pass before being detected. This shifted by varying amounts the apparent values of Q^2 and s, relative to the true values for the scattering reaction. Multiple scattering, finite target size, and wire chamber resolution had a somewhat similar effect. For each Q^2, s bin in the data we calculated[15] by Monte Carlo technique the true average Q^2 and s to use in plotting and fitting the multiplicity results for that bin.

The background from radiative elastic scattering was handled differently, however. We generated a Monte Carlo sample of such events, based on the known elastic cross section and the equivalent radiator approximation,[15] then propagated the outgoing electron and proton through our apparatus to determine the apparent Q^2 and s of the electron and the number of hadron latches set by the proton (usually one, but sometimes more or less, because of the processes to be

TABLE I. Running conditions and numbers of events.

Synchrotron energy (GeV)	7.0	11.5	11.5
Geometry	near	near	far
Electron scattering angles	9–20°	9–20°	14–25°
Incident electrons H target	4×10^{13}	11×10^{13}	70×10^{13}
D target	5×10^{13}	12×10^{13}	35×10^{13}
Accepted events H	5440	6588	8671
D	12 258	17 947	8348

described below). For each data bin in Q^2 and s this Monte Carlo hadron latch distribution, weighted by the expected number of radiative elastic events (up to 10%), was subtracted from the experimental data.

B. Unfolding procedure

The number of scintillator latches set in each event (minus one, for the electron) is a measure of the charged hadron multiplicity, but unfortunately it is not always a precise one. Accidental coincidences, δ rays, photon conversions, momenta below threshold, gaps in the scintillator array, and other processes discussed in detail below can cause the observed charged hadron multiplicity to be different from the true charged multiplicity in the deep-inelastic electron-proton collision. Suppose that for a given Q^2 and s bin the observed latch distribution is given by f_m ($m=0, 1, 2, \ldots$); that is, f_m is the fraction of events observed with $m+1$ latches set (including the electron). Let the true prong distribution be F_n ($n=1, 3, 5, \ldots$, odd because of charge conservation); that is, $F_n=\sigma_n/\sigma_{\text{tot}}$, the fractional cross section to produce n charged hadrons. Then formally we can write

$$f_m=\sum_n P_{mn}F_n, \tag{5}$$

where P_{mn} is the probability that an event of true multiplicity n will set m latches (plus one, for the electron). We need to know the P_{mn} for each Q^2, s bin in order to extract the desired F_n from the measured f_m.

C. Model

To get P_{mn} we need a model which tells how the n secondaries of a collision are distributed in momentum and angle. The model should conserve energy, momentum, and charge; it should predict momentum and angle distributions which agree with experimental data wherever available; it should contain no assumptions about multiplicities; and the F_n obtained by "inverting" the matrix equation (5) should not be sensitive to untestable details of the model.

We first simulated by the Monte Carlo technique electron scattering events, distributed as expected over the electron detection aperture. For each given charged hadron multiplicity n we selected at random (within limitations about to be described) the number of neutrals and the identity and three-momentum of charged and neutral

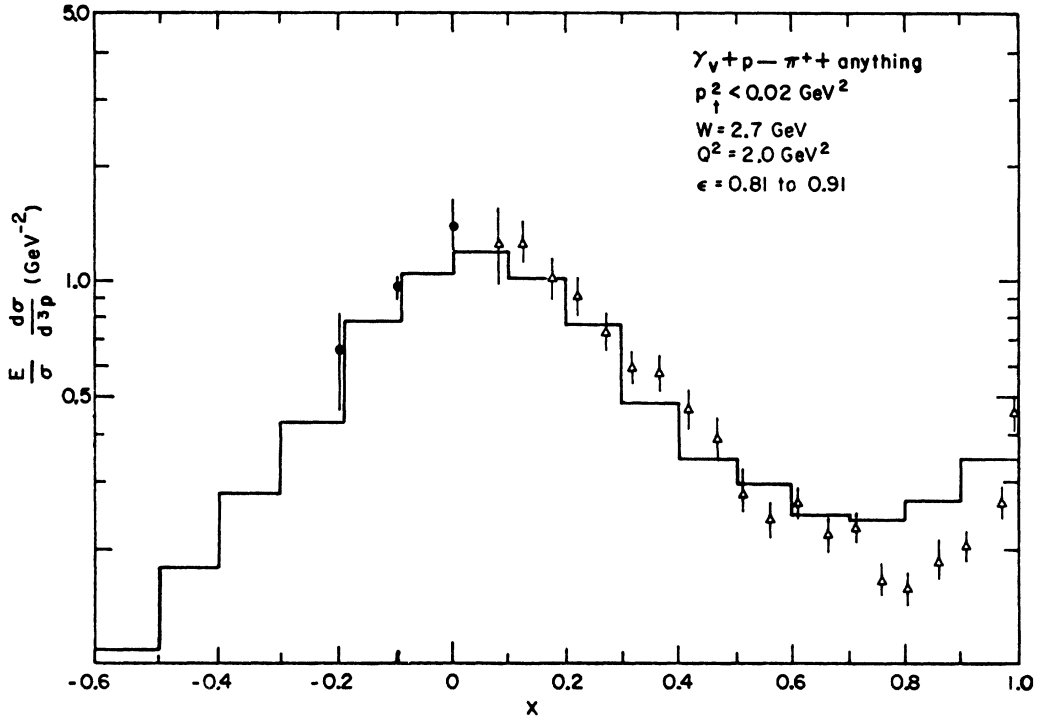

FIG. 4. Comparison of the Monte Carlo-generated distribution of longitudinal momentum for electroproduced π^+ (histogram) and experimental data (circles from Ref. 13, triangles from Ref. 24). Note that the Monte Carlo is integrated over all transverse momenta, while the data are for $p_t \approx 0$ only. The variable is $x=p_l^{\text{c.m.}}/p_{\text{max}}^{\text{c.m.}}$.

hadrons in the virtual-photon-plus-nucleon center-of-mass frame. This selection process is an adaptation of the method of Pène and Krzywicki.[16,17] The secondary momenta were chosen at random uniformly in momentum space, except that (a) each event was constrained to satisfy energy and momentum conservation, (b) transverse momenta were distributed as $\exp(-bp_t^2)$ with $b = 9$ GeV^2 for pions,[18] and $b = 3$ GeV^2 for nucleons,[19] (c) longitudinal momenta for outgoing nucleons were mainly in the backward hemisphere.[19,20] The number of π^0 was taken from a Poisson distribution with a mean at 0.4 times the number of π^-.[21] The average neutron/proton ratio in the final states was taken to be one.[22] No two-particle correlations were assumed; at the s values of this experiment correlations tend to be either kinematical consequences of energy-momentum conservation, or else correspond to resonance production. One example of the latter, ρ^0 production, is known[23] to be much less important in electroproduction above $Q^2 = 1.5$ GeV^2 than in photoproduction. No explicit account was taken of strange hadrons; for the purposes of this experiment they were assumed to behave like pions and nucleons on the average. In Figs. 4 and 5 we compare the inclusive longitudinal momentum spectra of our simulated events (relative probabilities of the various multiplicities n taken from our final results for F_n) with available electroproduction data.[20,23,24]

D. Multiplicity losses and gains

Each of the secondary particles, charged and neutral, in the simulated events was propagated through to the hadron detectors to determine the apparent experimental multiplicity m. In doing so, we took account of the following effects.[17]

(1) Gaps in the counter system. Final-state hadrons which escaped through the 3° forward cone, the backward 20° cone, and the 3.8 cm square hole above the target were not counted. This caused a loss of typically 5%.

(2) Two or more particles hitting the same scintillator. These were counted as one; the

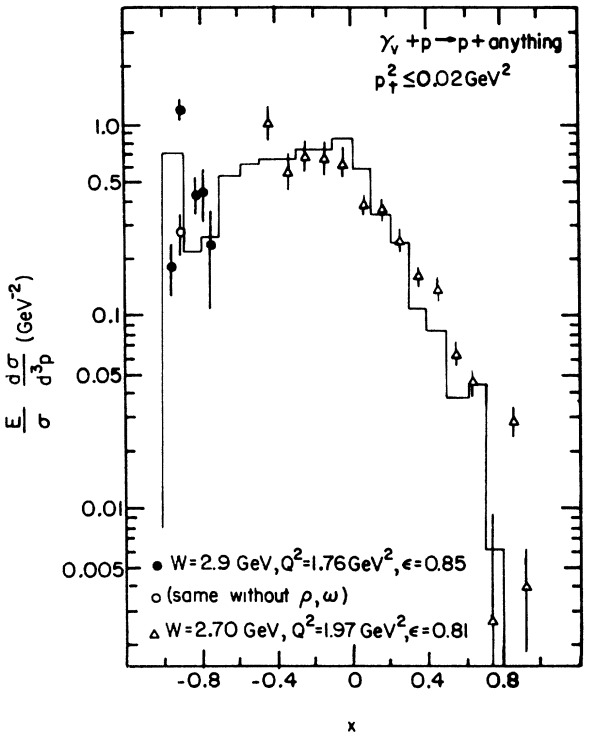

FIG. 5. Comparison of Monte Carlo-generated distribution of longitudinal momentum for electroproduced protons (histogram) and experimental data (circles from Ref. 23, triangles from Ref. 20). Note that the Monte Carlo is integrated over all transverse momenta, while the data are for $p_t \approx 0$ only. The variable is $x = p_l^{\text{c.m.}}/p_{\max}^{\text{c.m.}}$.

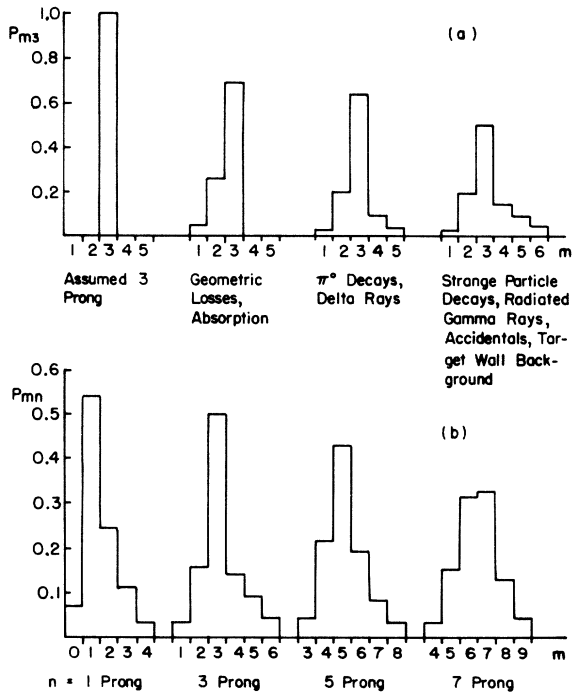

FIG. 6. (a) Plot of P_{mn} versus m for $n = 3$, at various stages of the Monte Carlo calculation, showing the cumulative effect of the multiplicity corrections. (b) Plot of P_{mn} versus m for $n = 1, 3, 5, 7$. Calculations are for the bin $\bar{Q}^2 = 2.3$ GeV^2, $\bar{s} = 9.6$ GeV^2. P_{mn} is the probability than an n-prong ep scattering event will be detected as an m-prong event.

loss averaged about 7%.

(3) Absorption. Slow particles, mainly protons backward in the center-of-mass frame, were ranged out in the 1.3 to 2.3 g/cm^2 of material between the production point in the hydrogen target and the scintillators. This loss amounted to about 5%.

(4) Conversion of γ's from π^0 decay. This was a significant effect, since there was about one π^0 per event on the average, and there was about 5% of the radiation length of material between target and detectors.

(5) δ rays and conversion of radiated γ rays. These effects were estimated using the appropriate electrodynamic cross sections.

(6) Charged decays of short-lived neutral strange particles. Following the somewhat arbitrary convention established by bubble chamber experimenters, we define the ρ^0 as two charged particles but the K^0 as a neutral particle. We therefore have to estimate the contribution to the observed charged multiplicity n from $K_S^0 \to \pi^+ + \pi^-$, $\Lambda \to p + \pi^-$, and so on. The data on electroproduction of neutral strange particles are rather sparse. In the μp bubble chamber experiment[9] 2% to 8% of the events have visible neutral strange particle decays. The yield seems to increase with s but appears to be independent of Q^2. If we assume a 5% probability of such a decay, coupled with an 80% chance of seeing both decay products, this leads to an average increase in n of 0.09.

(7) Accidental coincidences. For each simulated deep-inelastic scattering event we added a number of random hadrons according to a probability distribution in number and direction which was obtained from the observed fake triggers.

For a sample Q^2 and s bin Fig. 6(a) shows P_{mn} as a function of m for $n = 3$, after the various stages of the calculation. In Fig. 6(b) we plot the final P_{mn} as a function of m for $n = 1, 3, 5, 7$ for the same Q^2 and s bin.

E. Fitting

The matrix equation (5) is actually a set of linear equations (one for each $m = 0, 1, 2, \ldots$) in the unknowns F_n (one for each $n = 1, 3, 5, \ldots$), so that the system is overdetermined. It is "solved" for each Q^2, s bin by making a least-squares fit for the set of F_n that best satisfies (5) with the constraints that $\sum F_n = 1$ and $F_n \geq 0$. Figure 7 shows for several Q^2, s bins a comparison of the observed multiplicity distribution f_m, the derived true distribution F_n, and the fitted f_m obtained from $\sum P_{mn} F_n$. The average charged hadron multiplicity for each Q^2, s bin is calculated from $\bar{n} = \sum n F_n$; Table II lists the results.

It is interesting to note that the loss effects

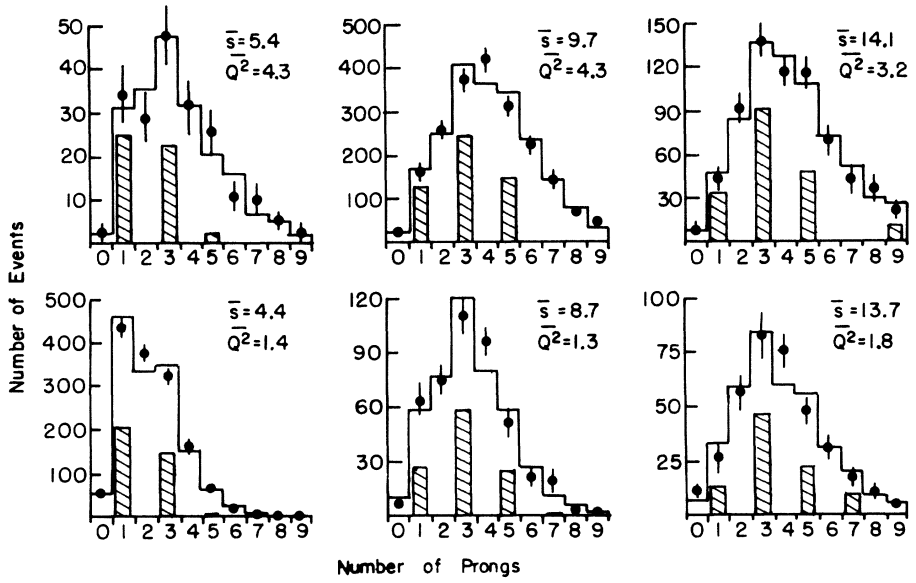

FIG. 7. *ep* multiplicity distributions for several Q^2, s bins. The data points with errors are the observed distributions f_m. The shaded bars show (with a factor of 4 reduction in vertical scale, for clarity) the fitted true multiplicity distributions F_n. The histogram is the predicted experimental distribution obtained from $\sum P_{mn} F_n$. The vertical scale is the number of events of each multiplicity.

TABLE II. Average charged hadron multiplicities $\bar{n}$ and fractional prong cross sections $F_n = \sigma_n/\sigma_{\text{tot}}$ measured in electron-proton inelastic scattering. Indicated errors are statistical only; systematic errors are about ±0.15 (see text).

s (GeV^2)	Q^2 (GeV^2)	ϵ	$\bar{n}$	F_1	F_3	F_5	F_7	F_9
2.90	1.44	0.94	1.28 ± 0.07	0.87 ± 0.03	0.13 ± 0.04	0.00 ± 0.02	0.00 ± 0.01	
3.05	2.18	0.91	1.32 ± 0.12	0.93 ± 0.05	0.05 ± 0.07	0.01 ± 0.04	0.01 ± 0.01	
3.32	3.03	0.89	1.47 ± 0.32					
4.04	4.75	0.88	1.67 ± 0.35					
3.94	6.13	0.84	1.77 ± 0.38					
3.80	7.98	0.75	2.56 ± 0.65					
4.41	1.41	0.87	1.91 ± 0.04	0.57 ± 0.02	0.40 ± 0.03	0.03 ± 0.02	0.00 ± 0.01	0.00 ± 0.01
4.56	2.25	0.83	2.01 ± 0.08	0.52 ± 0.04	0.45 ± 0.05	0.02 ± 0.03	0.00 ± 0.03	0.00 ± 0.02
5.24	3.12	0.89	1.98 ± 0.19	0.56 ± 0.07	0.41 ± 0.10	0.00 ± 0.06	0.02 ± 0.04	0.00 ± 0.03
5.52	4.85	0.82	2.15 ± 0.15	0.51 ± 0.06	0.43 ± 0.08	0.04 ± 0.06	0.02 ± 0.03	0.00 ± 0.01
5.41	6.17	0.77	1.60 ± 0.26	0.73 ± 0.10	0.23 ± 0.15	0.03 ± 0.12	0.00 ± 0.03	0.00 ± 0.05
5.36	7.77	0.68	2.53 ± 0.50					
6.27	1.35	0.74	2.59 ± 0.04	0.35 ± 0.02	0.53 ± 0.02	0.11 ± 0.02	0.01 ± 0.01	0.00 ± 0.01
6.91	2.38	0.81	2.54 ± 0.07	0.34 ± 0.02	0.56 ± 0.03	0.09 ± 0.03	0.01 ± 0.02	0.00 ± 0.01
7.24	3.16	0.83	2.58 ± 0.10	0.38 ± 0.03	0.45 ± 0.05	0.16 ± 0.04	0.00 ± 0.02	0.00 ± 0.01
7.54	4.62	0.74	2.75 ± 0.07	0.30 ± 0.02	0.54 ± 0.04	0.15 ± 0.04	0.00 ± 0.02	0.01 ± 0.01
7.40	6.15	0.65	2.68 ± 0.29	0.38 ± 0.05	0.44 ± 0.08	0.15 ± 0.07	0.04 ± 0.18	0.00 ± 0.16
6.57	7.58	0.62	3.07 ± 0.75					
8.31	1.26	0.48	3.09 ± 0.10	0.23 ± 0.03	0.52 ± 0.05	0.23 ± 0.05	0.02 ± 0.03	0.00 ± 0.01
9.56	2.35	0.76	3.17 ± 0.07	0.21 ± 0.02	0.52 ± 0.03	0.26 ± 0.03	0.01 ± 0.02	0.01 ± 0.01
9.85	3.31	0.69	3.26 ± 0.09	0.24 ± 0.02	0.41 ± 0.04	0.33 ± 0.05	0.00 ± 0.04	0.01 ± 0.02
9.79	4.41	0.62	3.11 ± 0.05	0.24 ± 0.02	0.48 ± 0.03	0.27 ± 0.03	0.01 ± 0.02	0.00 ± 0.01
9.81	5.96	0.52	3.15 ± 0.21	0.19 ± 0.05	0.54 ± 0.10	0.27 ± 0.17	0.00 ± 0.10	0.00 ± 0.02
11.21	1.73	0.64	3.47 ± 0.13	0.15 ± 0.03	0.48 ± 0.05	0.36 ± 0.06	0.01 ± 0.05	0.00 ± 0.03
11.52	2.22	0.62	3.51 ± 0.07	0.14 ± 0.02	0.50 ± 0.03	0.31 ± 0.04	0.03 ± 0.03	0.01 ± 0.01
12.16	3.34	0.52	3.55 ± 0.06	0.17 ± 0.01	0.47 ± 0.03	0.29 ± 0.04	0.07 ± 0.03	0.00 ± 0.02
12.06	4.28	0.45	3.53 ± 0.09	0.18 ± 0.02	0.47 ± 0.04	0.26 ± 0.06	0.08 ± 0.05	0.01 ± 0.02
10.68	5.39	0.44	3.31 ± 1.80					
13.70	1.83	0.54	3.67 ± 0.13	0.13 ± 0.03	0.51 ± 0.05	0.25 ± 0.06	0.11 ± 0.05	0.00 ± 0.03
13.95	2.51	0.46	3.77 ± 0.10	0.14 ± 0.02	0.49 ± 0.04	0.28 ± 0.05	0.05 ± 0.04	0.05 ± 0.02
14.26	3.24	0.38	3.44 ± 0.11	0.18 ± 0.03	0.51 ± 0.06	0.26 ± 0.07	0.01 ± 0.05	0.04 ± 0.02
13.80	3.97	0.31	3.27 ± 0.27	0.12 ± 0.07	0.68 ± 0.13	0.15 ± 0.17	0.05 ± 0.15	0.00 ± 0.08

(1, 2, and 3 in the above listing) very nearly balance the nonaccidental gains (4, 5, and 6), so that the uncorrected observed average multiplicity $\bar{m} = \sum m f_m$ minus the average multiplicity of the fake events $\bar{n}_{\text{fake}}$, is very nearly equal to the true average multiplicity $\bar{n}$ obtained by solving Eq. (5) and computing $\bar{n} = \sum n F_n$. In Q^2, s bins containing less than 50 actual events there are insufficient data to justify the full unfolding procedure. In those cases we have not obtained F_n but have instead approximated $\bar{n} = \bar{m} - \bar{n}_{\text{fake}}$ (corrected for the probability that an accidental and real will hit the same scintillator); any error we make in neglecting the corrections is negligible compared to the statistical error in $\bar{m}$.

It should be emphasized that, although we can correct the mean multiplicity and the prong distributions on the *average*, there is no way of correcting individual events for lost hadrons or additional spurious hadron counts. All events were treated uniformly in the analysis, without prejudice as to the likelihood of even or odd numbers m of hadrons or large or small m. At low beam intensities, where random coincidences did not contribute significantly, the evens ($m = 0, 2, 4...$) actually comprised about 40% of the events, rather independent of Q^2 and s.

F. Checks

It is obvious that we rely heavily on the procedure and parameters in our Monte Carlo simulation of the experiment. The fact that the least-squares fitting yielded acceptable χ^2 values is a necessary but not sufficient assurance that the P_{mn} matrix elements used were reasonable. We

have had to assume that the properties of our model of the particle ratios and inclusive momentum distributions, which correctly reproduce existing results in the $Q^2 = 2$ GeV^2 region (Figs. 4 and 5), can be extrapolated to high Q^2, where no such data exist.

The main corrections controlled by the transverse and longitudinal momentum distributions are the ranging out of slow protons, the conversion of γ's from π^0 decays, and the correction for two hadrons in one counter. We have checked the sensitivity of the Monte Carlo approach by varying the input parameters and observing the change in fitted mean multiplicities $\bar{n}$. For a sample Q^2, s bin Table III lists the partial derivatives of the fitted $\bar{n}$ with respect to the various input parameters.

The largest effect appears to be in the neutron/proton ratio. Because the protons often emerge backward in the virtual-photon-plus-proton center-of-mass system, they are relatively slow in the laboratory and often stop before reaching the detector. Fortunately, however, there is a minimum momentum that a spacelike photon can transfer to the proton, and this leads to a lower limit for the proton lab momentum. At low s all protons will have enough momentum to be detected regardless of their momentum distribution in the center-of-mass system. Here, where the $\pi^0 p$ and $\pi^+ n$ channels dominate, we can be rather sure of counting the charged hadron, whether it is a p or π^+, and therefore the uncertainty in the expected neutron/proton ratio has little effect on the low-s data. At higher s the higher multiplicities tend to dilute somewhat the effect of the loss of protons and the uncertainty in the neutron/proton ratio.

TABLE III. Partial derivatives of the fitted mean multiplicity $\bar{n}$ with respect to various parameters z assumed in the Monte Carlo calculation of the matrix elements P_{mn} (see text). Numerical values are quoted for *ep* scattering in the data bin $Q^2 = 2.3$ GeV^2, $s = 9.6$ GeV^2. The mean multiplicity for this bin is $\bar{n} = 3.17 \pm 0.07$.

Parameter	Assumed value z	$\partial\bar{n}/\partial z$
Neutron/proton ratio	1.0	−0.10
$p_t{}^2$ slope ($\pi^\pm$)	9 GeV^{-2}	0.02
$p_t{}^2$ slope (p)	3 GeV^{-2}	0.01
γ conversion probability	0.04	1.33
Pair/Compton ratio	1.0	−0.01
Strange particle decays	0.05	−1.8
π^0/π^- ratio	0.4	−0.04

We have required that the fitted $\bar{n}$ found with different absorber configurations, each analyzed with its appropriate P_{mn}, be consistent within statistical errors. In addition to the aluminum vacuum chamber wall, we have used the standard polyethylene absorber, extra aluminum, lead plus polyethylene, and finally, no extra absorber. The lead caused a large increase in the probability of π^0 conversion. We found consistency only when $\bar{n}(\pi^0)/\bar{n}(\pi^-)$ was 0.40 ± 0.25, as opposed to the ratio 1.0 expected from simple isospin arguments. Although our uncertainty on this measurement is large, we are in agreement with photoproduction data[21] at 6 GeV, giving ratio values between 0.25 and 0.5. This same photoproduction experiment[21] indicates a flatter $p_t{}^2$ distribution for the π^0 relative to that for charged pions. Their slope parameter is typically $b = 4$ GeV^2. We have generated events using this slope also, and have obtained negligible variation in the fitted multiplicities. Even if the dynamic suppression of large transverse momentum secondaries is removed from the model (that is, if we use the James method instead of the method of Pène and Krzywicki[16]), the results for $\bar{n}$ still turn out to be essentially the same, within experimental error.

The Monte Carlo calculation that gives the matrix elements P_{mn} also predicts the distribution of counts among the 68 scintillators, once the relative weights F_n of various multiplicities are determined. This enables us to make a sensitive test of the validity of the model, even at higher Q^2 where no other data are available. The comparison is discussed in detail in Sec. X below. For now, we note that there are no significant differences between the Monte Carlo and experimental angular distributions throughout our range of Q^2 and s.

Since the accidental correction was rather large (up to 30%), we required that the results of the analysis be independent of the beam intensity used in the data taking. This was confirmed within counting statistics over a range of incident electron intensities from 6×10^7/sec to 10^9/sec.

The uncertainties listed in Table II are statistical counting errors propagated through the fitting procedure. The systematic error in the mean multiplicity, corresponding essentially to an overall normalization uncertainty, is estimated to be about 0.15, perhaps somewhat larger at the lowest s range.

VII. MULTIPLICITY ANALYSIS: NEUTRON TARGET

The distribution of multiplicities in electron-neutron scattering was extracted from the deu-

terium-target data using the relation

$$f_m^{(d)} = \frac{\sigma_p}{\sigma_p + \sigma_n} \sum_{m'} P_{mm'}^{(p)} F_{m'}^{(p)} + \frac{\sigma_n}{\sigma_p + \sigma_n} \sum_{m'} P_{mm'}^{(n)} F_{m'}^{(n)}, \tag{6}$$

where $f_m^{(d)}$ is the observed charged prong distribution from deuterium (fraction of events with $m = 0, 1, 2, \ldots$ charged hadron latches), $F_m^{(p)} = \sigma_m(ep)/\sigma_{\text{tot}}(ep)$ $(m = 1, 3, 5, \ldots)$, $F_m^{(n)} = \sigma_m(en)/\sigma_{\text{tot}}(en)$ $(m = 0, 2, 4, \ldots)$. σ_p and σ_n are the measured[25] ep and en cross sections at the appropriate Q^2 and s; we have used the parametrization $\sigma_n = (1 - 0.75x)\sigma_p$ with $x = Q^2/2M\nu$. $P_{mm'}^{(p)}$ and $P_{mm'}^{(n)}$ are the Monte Carlo-generated probabilities (for the ep and en scatterings, respectively) that transform the true prong distributions into the experimentally observed latch distributions. For each Q^2 and s bin, Eq. (6) was solved for $F_m^{(n)}$ by least squares fitting. The already determined $F_{m'}^{(p)}$ were interpolated slightly in Q^2 and s to correspond to the average Q^2 and s values appropriate to the deuterium data.

The analysis was otherwise the same as in the ep scattering case, except for corrections to account for three additional effects.

(1) Spectator proton. In an en collision the proton will be detected as if it were a final state hadron, provided it has sufficient range to reach the scintillators. According to the momentum spectrum of nucleons bound in the deuteron,[26] about 5% of the spectator protons have sufficient momentum (about 260 MeV/c) to be detected. Hence this contribution to the observed mean multiplicity is about 0.05.

(2) Fermi momentum. The momentum of the target nucleon causes a shift in the s of the virtual-photon-plus-nucleon collision; it has no

TABLE IV. Average charged hadron multiplicities $\bar{n}$ and fractional prong cross sections $F_n = \sigma_n/\sigma_{\text{tot}}$ measured in electron-neutron inelastic scattering. Indicated errors are statistical only; systematic errors are about ±0.3 (see text).

s (GeV^2)	Q^2 (GeV^2)	$\bar{n}$	F_0	F_2	F_4	F_6	F_8
3.13	1.43	0.99 ± 0.19					
3.25	2.16	0.51 ± 0.37					
3.59	2.99	0.91 ± 0.89					
4.63	4.70	0.33 ± 1.14					
4.46	6.00	3.43 ± 1.41					
4.48	7.87	−0.05 ± 2.67					
4.58	1.38	1.66 ± 0.10	0.23 ± 0.02	0.70 ± 0.05	0.06 ± 0.07	0.00 ± 0.03	0.00 ± 0.02
4.87	2.24	2.07 ± 0.26	0.13 ± 0.04	0.77 ± 0.11	0.05 ± 0.13	0.04 ± 0.07	0.02 ± 0.04
5.63	3.05	1.82 ± 0.68	0.45 ± 0.15	0.36 ± 0.25	0.02 ± 0.31	0.17 ± 0.23	0.00 ± 0.06
5.95	4.68	2.32 ± 0.39	0.22 ± 0.09	0.51 ± 0.17	0.21 ± 0.19	0.00 ± 0.13	0.06 ± 0.06
5.92	6.03	3.90 ± 1.22	0.00 ± 0.11	0.31 ± 0.43	0.51 ± 0.74	0.10 ± 0.52	0.08 ± 0.10
5.93	7.68	2.07 ± 1.64					
6.45	1.34	2.51 ± 0.09	0.08 ± 0.01	0.64 ± 0.04	0.24 ± 0.06	0.05 ± 0.04	0.00 ± 0.01
7.32	2.36	2.96 ± 0.19	0.07 ± 0.03	0.52 ± 0.07	0.31 ± 0.09	0.08 ± 0.07	0.03 ± 0.04
7.64	3.10	2.97 ± 0.22	0.10 ± 0.03	0.36 ± 0.09	0.51 ± 0.14	0.00 ± 0.11	0.02 ± 0.05
7.88	4.55	2.80 ± 0.18	0.08 ± 0.02	0.48 ± 0.07	0.39 ± 0.09	0.05 ± 0.06	0.00 ± 0.03
7.76	6.08	3.36 ± 0.61	0.00 ± 0.05	0.32 ± 0.18	0.68 ± 0.29	0.00 ± 0.24	0.00 ± 0.14
6.99	7.45	−2.27 ± 2.40					
8.79	1.32	2.42 ± 0.20	0.09 ± 0.03	0.68 ± 0.08	0.20 ± 0.11	0.00 ± 0.09	0.03 ± 0.04
9.78	2.32	3.64 ± 0.13	0.03 ± 0.01	0.34 ± 0.04	0.45 ± 0.07	0.16 ± 0.07	0.03 ± 0.04
10.02	3.24	3.42 ± 0.20	0.03 ± 0.02	0.46 ± 0.06	0.33 ± 0.11	0.14 ± 0.11	0.04 ± 0.06
10.07	4.37	3.57 ± 0.16	0.06 ± 0.02	0.41 ± 0.05	0.28 ± 0.08	0.18 ± 0.09	0.07 ± 0.04
10.00	5.90	3.92 ± 0.58	0.03 ± 0.04	0.18 ± 0.16	0.60 ± 0.29	0.20 ± 0.36	0.00 ± 0.20
12.06	1.81	3.88 ± 0.25	0.00 ± 0.02	0.36 ± 0.08	0.33 ± 0.12	0.28 ± 0.13	0.01 ± 0.05
11.83	2.23	4.06 ± 0.13	0.01 ± 0.01	0.35 ± 0.04	0.34 ± 0.06	0.19 ± 0.07	0.10 ± 0.04
12.30	3.28	3.81 ± 0.13	0.05 ± 0.01	0.32 ± 0.04	0.36 ± 0.07	0.23 ± 0.06	0.04 ± 0.03
12.31	4.23	3.77 ± 0.23	0.05 ± 0.02	0.30 ± 0.07	0.40 ± 0.11	0.24 ± 0.11	0.02 ± 0.07
11.56	5.51	11.27 ± 4.17					
13.93	1.77	3.90 ± 0.24	0.00 ± 0.02	0.32 ± 0.08	0.54 ± 0.12	0.00 ± 0.13	0.14 ± 0.07
14.16	2.39	3.62 ± 0.17	0.03 ± 0.02	0.44 ± 0.05	0.23 ± 0.08	0.29 ± 0.07	0.01 ± 0.04
14.26	3.18	3.94 ± 0.22	0.05 ± 0.03	0.32 ± 0.08	0.24 ± 0.12	0.38 ± 0.11	0.01 ± 0.04
13.94	3.89	3.67 ± 0.56	0.00 ± 0.05	0.35 ± 0.19	0.51 ± 0.31	0.08 ± 0.25	0.06 ± 0.07

effect on Q^2. The s shift was taken into account by including the nucleon motion in the electron scattering Monte Carlo calculation. For each Q^2, s bin in the data we calculated the true average s to use in plotting and fitting the results for that bin.

(3) Final-state interactions. Collisions between the electroproduced hadrons and the spectator nucleon have an effect on the observed multiplicity which is difficult to evaluate reliably. We have made a rough estimate[27] based on the deuteron wave function,[26] known hadronic cross sections and multiplicities, and a plausible guess at the spatial development of the electroproduction multiplicity at small distances. The result implies a correction to the *en* multiplicity equal to -0.3, varying only slightly with Q^2 and s. Since this estimate is probably only good to within a factor of 2, we have not made the correction in our data.

Table IV lists the results of the fitting for $F_m^{(n)}$, and the corresponding mean multiplicities. The errors indicated are the statistical uncertainties propagated through the fitting procedure. We estimate a common systematic error of 0.3 in the average *en* multiplicity, perhaps somewhat larger at the lowest s range.

VIII. MULTIPLICITY RESULTS: PROTON TARGET

A. Mean multiplicities

Figure 8 shows the corrected charged hadron multiplicities in ep scattering, plotted as a function of Q^2 for six different fixed s values. In order to make this plot we have interpolated the multiplicity data (Table II) to nearby fixed s values, using the slopes obtained from a best fit to the form $\bar{n}(s, Q^2) = a + b \ln s$ (see discussion below). Photoproduction data[28] and low-Q^2 electroproduction data from DESY[8] and SLAC[9] track-chamber experiments are also included in Fig. 8 for comparison. Where our data overlap the other electroproduction data the agreement is generally satisfactory, except at the lowest s range, where the $\bar{n}$ obtained in this experiment appears to be significantly lower than reported for the DESY streamer chamber experiment.[8]

The three experiments need not agree, however. Since they obtain overlapping Q^2 and s values

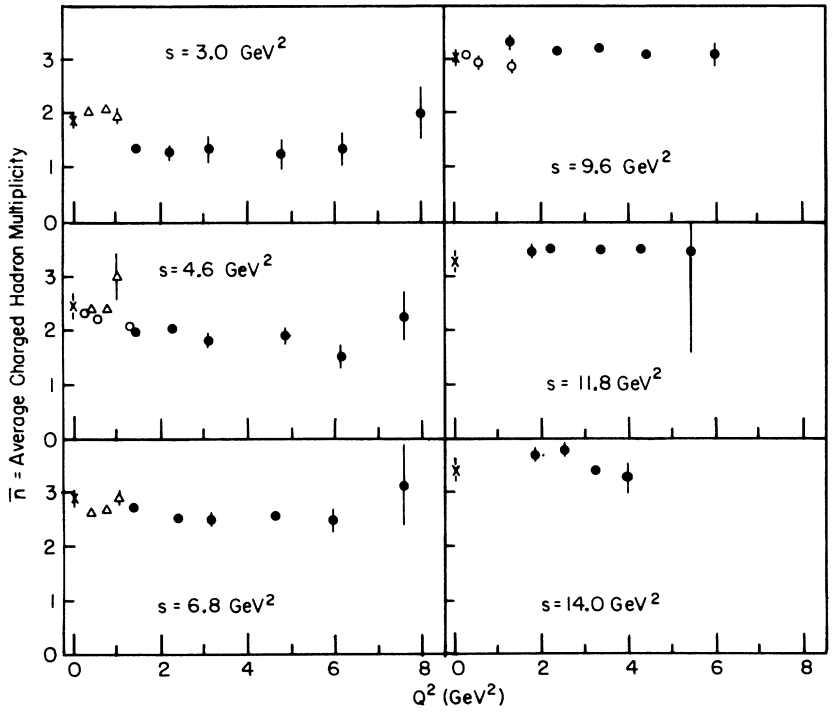

FIG. 8. Average charged hadron multiplicity in ep scattering as a function of Q^2 for six ranges of s. Dark circles represent data from this experiment, triangles are DESY data (Ref. 8), open circles are SLAC data (Ref. 9), and crosses are photoproduction data (Ref. 28). Data have been interpolated to the appropriate s values for comparison. The indicated error bars for this experiment represent statistical errors only (see text).

with different incident lepton energies, they can involve different values for the virtual-photon polarization parameter. If the average multiplicity produced by the transverse and longitudinal components were unequal, the three experiments could appear to be inconsistent. One could, for example, explain the discrepancies at $s = 9.6$ GeV^2 by supposing that transverse photons produce higher multiplicities than longitudinal photons. At the present state of the data, however, this speculation should probably not be taken seriously.

The most important result is the fact that we see little or no Q^2 dependence of $\bar{n}(s, Q^2)$ at fixed s, over a rather wide range of Q^2. At low s there is a slight decrease in $\bar{n}$ as Q^2 increases from 0 to 1.5 GeV^2. This can be explained by two effects. First, the diffractive channels ($\rho^0 p$, ωp, ϕp, for example) are three-prong topologies, and are known[23] to contribute a decreasing fraction of the total virtual-photon-plus-proton cross section as Q^2 increases. Second, the relative contribution of single pseudoscalar mesons, mainly by the longitudinal virtual-photon polarization component, tends to increase with Q^2 (see Ref. 29) and causes an increase in the one-prong fraction. After this transition effect from photoproduction to $Q^2 = 1.5$ GeV^2 the average multiplicity at higher Q^2 becomes essentially independent of Q^2 (at fixed s).

Over the kinematic range of our experiment our best fit to the charged hadron multiplicity in ep scattering is

$$\bar{n}(s, Q^2) = (-0.40 \pm 0.03) + (1.61 \pm 0.04)\ln s + (-0.11 \pm 0.03)\ln Q^2 \quad (7)$$

(errors are statistical). The χ^2 of this fit is 1.0 per degree of freedom. A simple $\ln s$ behavior gives the fit

$$\bar{n}(s, Q^2) = (-0.37 \pm 0.07) + (1.55 \pm 0.04)\ln s, \quad (8)$$

with $\chi^2 = 1.3$ per degree of freedom, only slightly worse than our best fit. Note that scaling in multiplicity would require the coefficients of the $\ln s$ and $\ln Q^2$ terms to be comparable in magnitude and opposite in sign. Such scaling behavior[30] in ω, ω', or ω_w is clearly incompatible with our data. The intuitive parton model suggests[5] the following form for the mean multiplicity:

$$\bar{n}(s, Q^2) = C_0 + C_h \ln s + (C_{e\bar{e}} - C_h)\ln Q^2, \quad (9)$$

where C_h is the same as the corresponding coefficient in hadronic collisions and $C_{e\bar{e}}$ is the coefficient of $\ln s$ for the charged hadron multiplicity in $e\bar{e}$→hadrons. Using our best-fit parameters, we find $C_h = 1.61 \pm 0.04$ and $C_{e\bar{e}} = 1.50 \pm 0.06$. These are to be compared with about 1.45 and 1.42 for hadronic collisions[31] and for e^+e^-,[32] respectively. A fit to a form similar to that suggested by the pulverization model[3] yields

$$\bar{n}(s, x) = (-2.8 \pm 0.1) + (3.53 \pm 0.05)(s - M^2)^{\alpha(x)}, \quad (10)$$

with

$$\alpha(x) = (0.25 \pm 0.05) + (-0.04 \pm 0.02)x.$$

Note that the x dependence of the exponent is zero or slightly negative, in contrast to the theoretical expectation.

B. Multiplicity distributions

Besides the mean, we can look at the next higher moment of the multiplicity distribution. We define a measure of dispersion

$$f_2 = \overline{n^2} - \bar{n}^2 - \bar{n} = \sum n^2 F_n - \left(\sum n F_n\right)^2 - \sum n F_n. \quad (11)$$

An independent emission model leading to a Poisson distribution for F_n would predict $f_2 = 0$. Because of the correlated errors in our fitted F_n data, it is difficult to obtain accurate values of f_2 from this experiment. Over our Q^2 and s range we observe f_2 varying between -0.5 and -1.0 with a typical uncertainty of ± 0.5. This consistent with results obtained in hadronic collisions[31] at similar energies.

Koba, Nielsen, and Olesen[33] have suggested that at very high s the function $\bar{n}F_n$ should be a universal function of $n/\bar{n}$. Although this is not

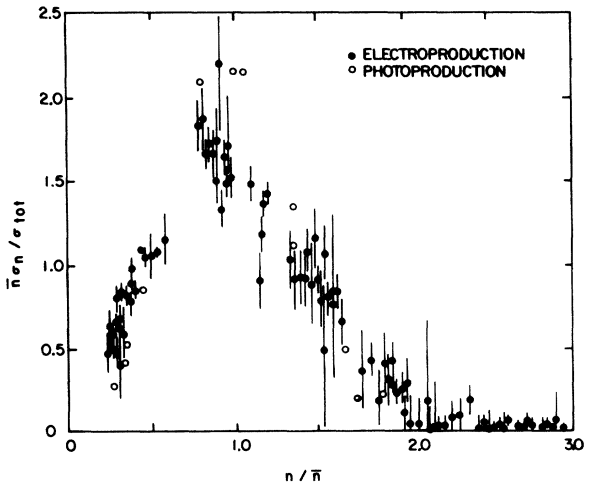

FIG. 9. Scaled multiplicity distributions from this experiment and photoproduction (Ref. 28). The data would be on a single smooth curve if KNO scaling (Ref. 33) were obeyed.

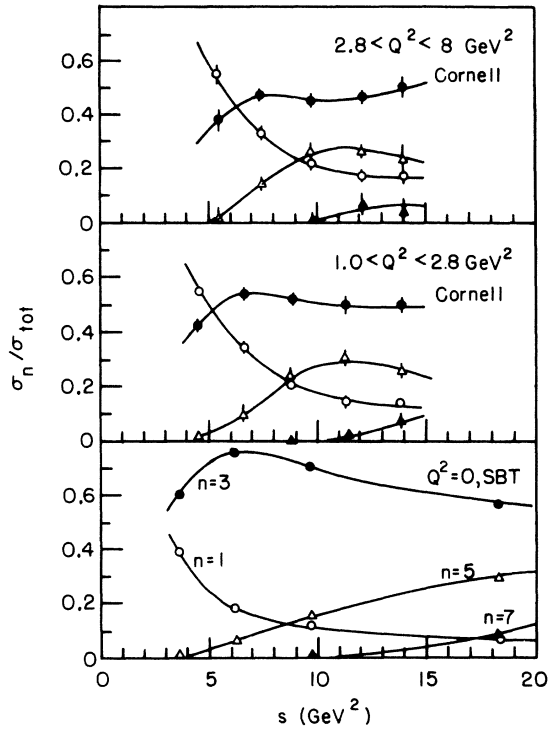

FIG. 10. Relative topological cross sections for $\gamma + p$, as a function of s, for real photons (Ref. 28) and virtual photons (this experiment) in two ranges of Q^2. The curves are drawn only for ease in distinguishing the points and have no theoretical significance.

expected to be true in our s range, we plot our data in this scaling form in Fig. 9. Photoproduction data[28] are also included for comparison. Our electroproduction data seem to be compatible with a single curve, but the three-prong photoproduction points are considerably above the curve. This may be the effect of the vector meson channels in photoproduction.

C. Relative topological cross sections

Figure 10 shows the fitted relative prong cross sections $F_n = \sigma_n/\sigma_{\text{tot}}$ in electroproduction, compared with photoproduction data.[28] Our data (Table II) have been combined into two Q^2 ranges with the division at $Q^2 = 2.8$ GeV^2. One sees very little difference between the electroproduction data at low and high Q^2. The one-prong events are decreasing while the five- and seven-prong events are increasing with increasing s. The three-prong fraction shows little variation above $s = 7$ GeV^2. The differences between electroproduction and photoproduction are significant, however. In photoproduction, the three-prong final state is much more important and the one-prong final state is smaller relatively than in electroproduction. This provides, in fact, a confirmation of our explanation of the low-Q^2 decrease in the average multiplicity.

In Fig. 11 we plot the Q^2 dependence of $\sigma_n/\sigma_{\text{tot}}$ at constant s. The data at $\bar{s} = 6.8$ GeV^2 are compared

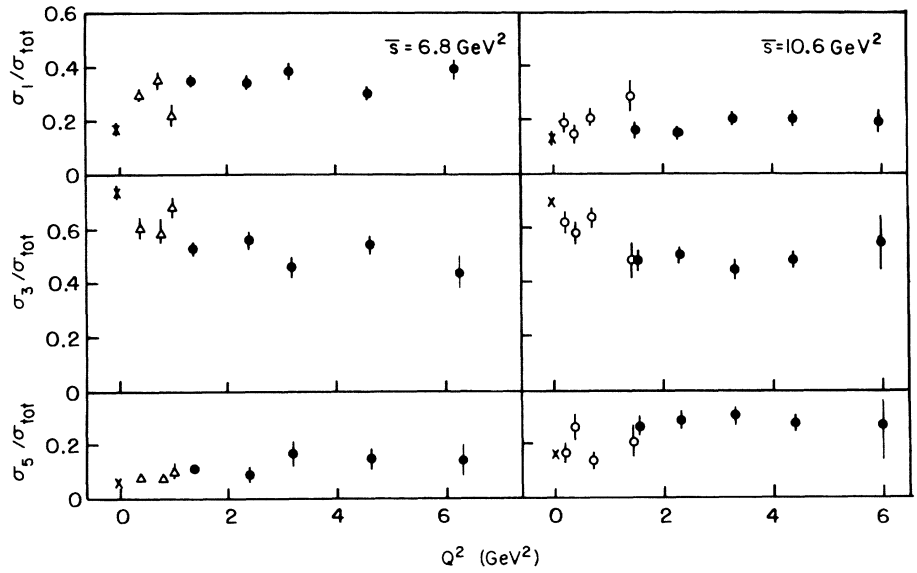

FIG. 11. Relative topological cross sections in ep scattering as a function of Q^2, for two ranges of s. The data references are the same as for Fig. 8.

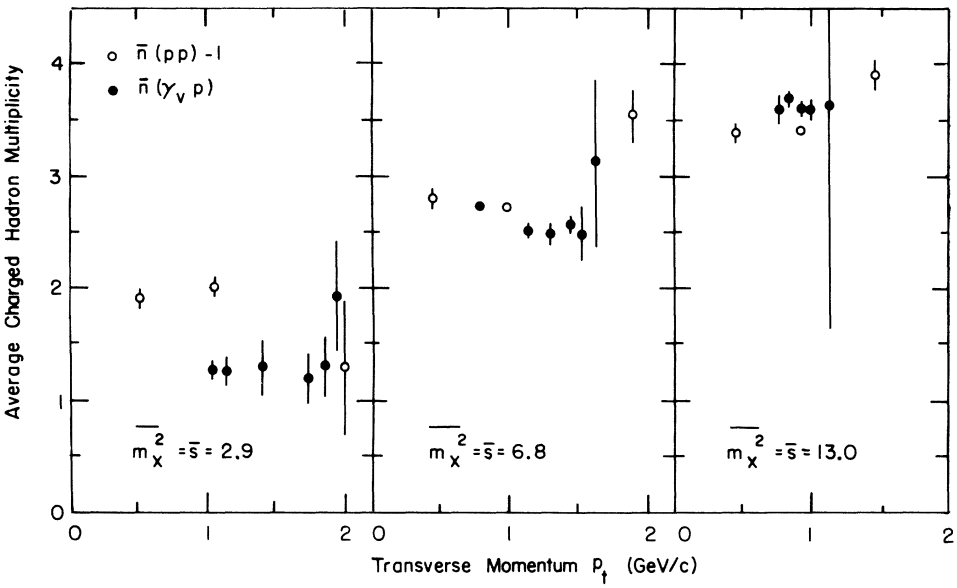

FIG. 12. A comparison of the dependence of associated multiplicity as a function of m_X^2 and p_t for $pp \to pX$ (open circles, Ref. 35) and $ep \to eX$ (dark circles, this experiment). The mass squared of the state X, m_X^2, is the same variable as our s; p_t is related to Q^2 (see text).

with the DESY streamer chamber data,[8] while we combine our $\bar{s} = 9.6$ and 11.6 GeV^2 data to compare with the SLAC bubble chamber results.[9]

D. Comparison with $pp \to pX$

Recently, several groups have studied associated multiplicities in hadron collisions. Bøggild *et al.*[34] have reported data for $pp \to hX$, where h includes p, Λ, π^-, and K^0, in a hydrogen bubble chamber. Ramanauskas *et al.*[35] have studied $pp \to pX$ using a forward spectrometer for the outgoing proton and observing the charged multiplicity of X in a cylindrical spark chamber enclosing the target. They investigate the dependence of $\bar{n}_X$ on the transverse momentum p_t of the proton and the mass-squared M_X^2 of the state X. This latter experiment is in fact a rather close analog of our electroproduction experiment, with the incident and final electrons replaced by protons. The relation between the variables we use is

$$M_X^2 = s, \qquad p_t^2 \approx (E'/E)Q^2 \text{ (in the small-angle limit).} \tag{12}$$

Ramanauskas *et al.* have reported[35] an increase in $\bar{n}_X(M_X^2, p_t)$ with increasing p_t at fixed M_X^2. In Fig. 12 our ep data are compared with the pp data over the M_X^2 range where they overlap. The

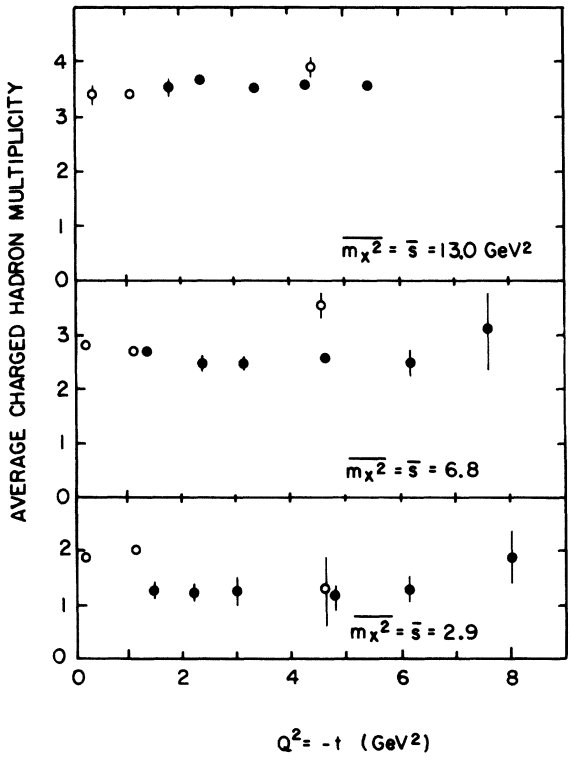

FIG. 13. The data of Fig. 12 replotted against Q^2.

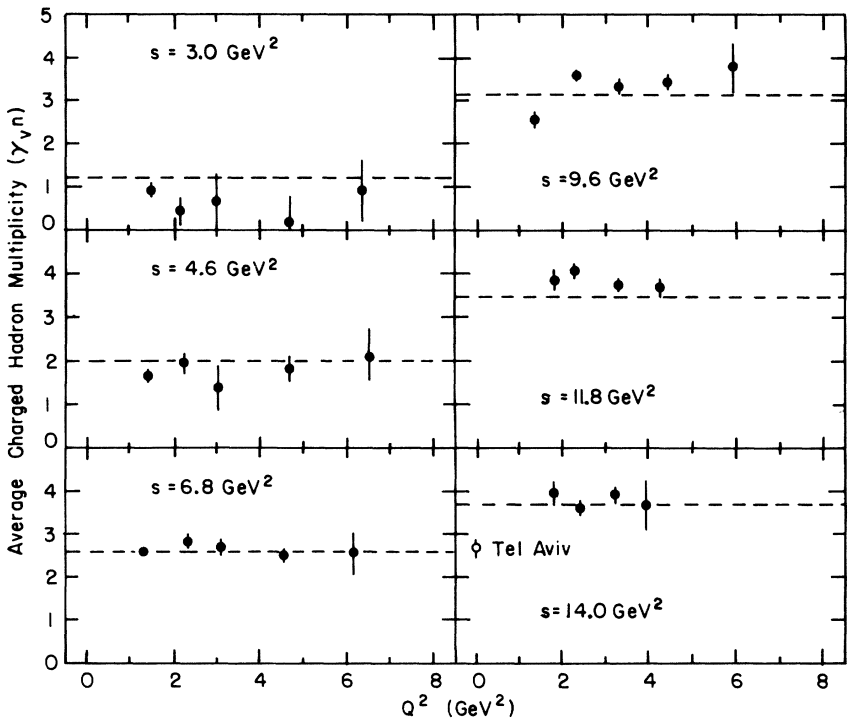

FIG. 14. Average charged hadron multiplicity in *en* scattering as a function of Q^2 for six ranges of s. The point marked "Tel Aviv" is a photoproduction measurement (Ref. 36). The dashed lines show the average trend of the *ep* data (from Fig. 8). The indicated error bars for this experiment represent statistical errors only (see text).

most important observation to make is that the *ep* and *pp* multiplicity data appear almost identical. *A priori*, one might expect the two processes to be completely unrelated. Our data are not inconsistent with the rise in multiplicity they report at high p_t, since it occurs at a p_t which is at the end of our range, where the statistical accuracy is marginal. Although the *pp* experiment has a slightly larger transverse momentum range than the *ep* data, the situation is reversed if the data are plotted (Fig. 13) in four-momentum transfer squared. We definitely do not observe their rise in multiplicity at a comparable Q^2. If the same multiplicity rise mechanism occurs in *ep* scattering, it would suggest that p_t is a more useful variable than Q^2, One can of course associate a p_t dependence with its conjugate coordinate, impact parameter.

IX. MULTIPLICITY RESULTS: NEUTRON TARGET

The results for the charged hadron mean multiplicity in *en* scattering are shown in Fig. 14, plotted versus Q^2 for six intervals in s. For comparison we have indicated our average *ep* multiplicity (from Fig.8) as a horizontal dashed line at each s value, since there is no significant Q^2 dependence. Again in the electron-neutron case we see no appreciable dependence of $\bar{n}(s, Q^2)$ on Q^2 in the range of our data. Furthermore, except at the lowest s, the multiplicities produced from the neutron and proton are essentially the same.

The only other comparable experiment is a photoproduction deuterium bubble chamber experiment[36] at $s = 15$ GeV^2. Their result is that the γn multiplicity is 0.9 ± 0.3 lower than the γp multiplicity. An estimate had to be made for the unseen contribution of $\gamma n \to 0$ prongs. Their estimate, $\sigma_0/\sigma_{tot} = 0.10$, seems anomalously high in light of our data (see Fig. 15); this may help to account for the low mean multiplicity.

The relative topological cross sections, as a function of s for two ranges in Q^2, are shown in Fig. 15. The high and low Q^2 data are similar except at the lowest s where we find the two-prongs decreasing while the zero-prongs increase with increasing Q^2. The general trends with increasing s for the 0, 2, 4, and 6 prong contributions follow the corresponding 1, 3, 5, and 7 prong contributions in the *ep* case (Fig. 10).

The photoproduction data[36] are also shown in Fig. 15 for comparison. The prong cross sections

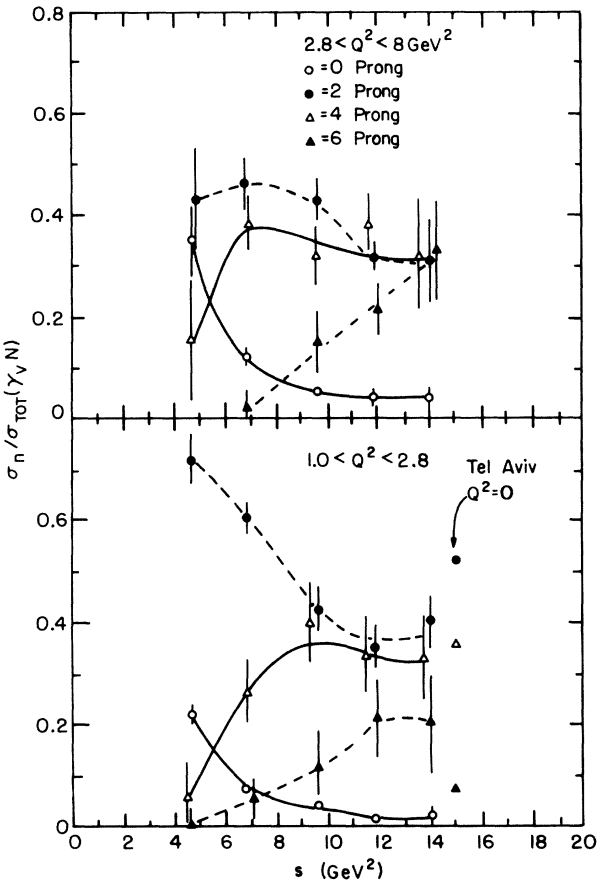

FIG. 15. Relative topological cross sections for $e+n$, as a function of s for two ranges of Q^2. The data marked "Tel Aviv" came from a photoproduction experiment (Ref. 36). The curves have no theoretical significance.

were calculated by subtracting the γp cross sections from the γd cross sections and correcting for unseen proton spectators. As expected from the Q^2 dependence of vector meson electroproduction, the two-prong contribution (containing $n\rho^0$, $n\omega$, $n\phi$) is considerably higher in photoproduction.

Since in the Q^2 range between 1.5 and 8 GeV^2 there seems to be no Q^2 dependence of $\bar{n}(s, Q^2)$ either for ep or en scattering, we average over Q^2 and compare the s dependences in Fig. 16. We also show for comparison the mean charged hadron multiplicities in γp,[28] $\pi^{\pm}p$,[37] e^+e^-,[32] $\bar{p}p$,[38] and the associated charged multiplicity in $pp \to pX$ (see Ref. 35) (averaged over p_t). The similarity in the multiplicities produced in these rather diverse processes, covering six orders of magnitude in cross section, is rather remarkable. For s above about 6 GeV^2 there seems to be little or no dependence on the identity of the colliding particles or on how far off the mass shell (Q^2) they are.

X. ANGULAR DISTRIBUTIONS

A. Angular variables

Although the primary purpose of this experiment was to measure the charged hadron multiplicities, our experimental apparatus also allowed a low-resolution study of the angular distributions of the produced hadrons. Since there was no momentum analysis or particle identification, we cannot determine rapidity, x, or p_t, or even transform to the center of mass. For high energy ($\beta \approx 1$) particles the laboratory frame rapidity

$$y = \tfrac{1}{2} \ln\left(\frac{E+p_l}{E-p_l}\right) \tag{13}$$

can be approximated by

$$\eta = -\ln\tan(\theta/2), \tag{14}$$

which depends only on the measured laboratory angle θ of the particle. This pseudorapidity (with θ defined relative to the virtual photon axis) provides a useful approximation for pions, even for the energies in our experiment. However, it is rather misleading for slow protons. In fact a proton emitted backward in the center-of-mass system will have the same η as a pion in the central region. Hence, we cannot expect to explore the rapidity distribution in any detail.

The azimuthal angle ϕ of the produced hadrons relative to the virtual photon axis (ϕ is zero in the electron scattering plane on the incident beam side of the virtual photon line) is, however, unambiguous and serves as a useful variable for this experiment.

B. Unfolding procedure

The main difficulty in obtaining distributions in η and ϕ from the data is the fact that the large electron aperture in momentum and angle allowed a wide range of possible virtual photon directions, so that the hadron scintillators did not subtend fixed angular ranges even in the laboratory frame.

The analysis scheme was a variation of that used for multiplicities. Bins in η and $|\phi|$ were defined, taking advantage of the required up-down symmetry in ϕ. Scattering events were simulated in a Monte Carlo calculation, with electrons distributed as expected over the spectrometer aperture and hadrons selected uniformly over a given bin in η and $|\phi|$. The hadrons were then propagated to the counter and the counters struck were noted. This then gave us P_{ij}^k, the probability that a hadron emitted in the ith inter-

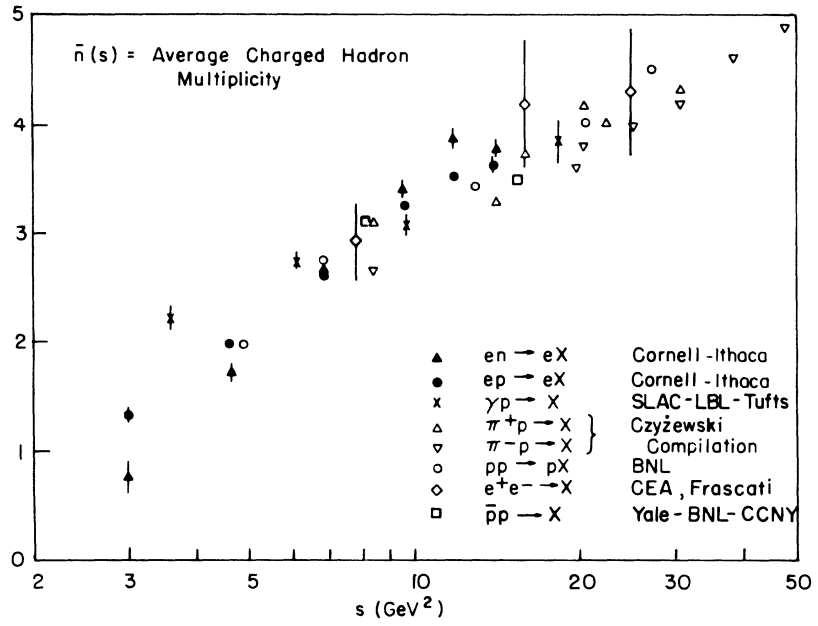

FIG. 16. The s dependence of the average charged multiplicity of the state X in the reactions $ep \to eX$ and $en \to eX$ (this experiment), $\gamma p \to X$ (Ref. 28), $\pi p \to X$ (Ref. 37), $pp \to pX$ (Ref. 35), $e^+e^- \to X$ (Ref. 32), and $\bar{p}p \to X$ (Ref. 38). In each case s is the center-of-mass energy squared of the state X. The data of this experiment and of Ref. 35 have been averaged over Q^2.

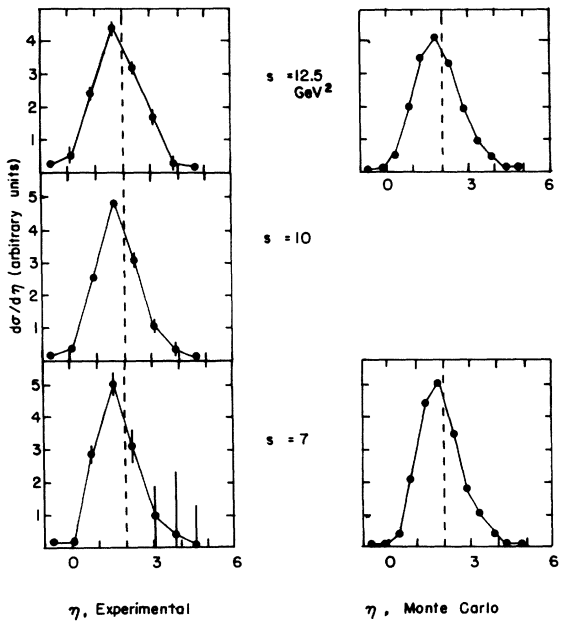

FIG. 17. Inclusive distributions of ep electroproduced hadrons in pseudorapidity, $\eta = -\ln\tan(\theta_{\rm lab}/2)$ at fixed $Q^2 = 2.5$ GeV^2, and several s values. The vertical scale is proportional to the virtual-photon-plus proton differential cross section $d\sigma/d\eta$; $\theta_{\rm lab}$ is measured with respect to the virtual-photon direction. Experimental and simulated data are compared (see text).

val of η and the jth interval of $|\phi|$ will hit the kth scintillator. The observed latch distribution f_k (with accidentals subtracted, using the fake events) was related to the desired η and $|\phi|$ distribution F_{ij} according to

$$f_k = \sum_{i,j} P_{ij}^k F_{ij} \tag{15}$$

In order to limit the number of independent quantities to be fitted, we made the approximation that the η and $|\phi|$ distributions factorized; thus $F_{ij} = a_i b_j$. The system of equations (15) was solved by finding the set of a_i, b_j which satisfied (15) with minimum χ^2. This was repeated for several Q^2, s bins (fewer and larger than those used in the multiplicity analysis).

In generating the probabilities P_{ij}^k we did *not* take into account the loss and gain effects numbered (2) through (6) in Sec. VID above. Such effects are, however, not expected to produce significant distortions of the η, ϕ distributions.

C. Pseudorapidity distributions

The η spectra for secondaries in ep scattering, arbitrarily normalized, are presented in Figs. 17 and 18. The predictions of the Monte Carlo model [including loss and gain effects (2) through (6)] used in the multiplicity analysis (see Sec.

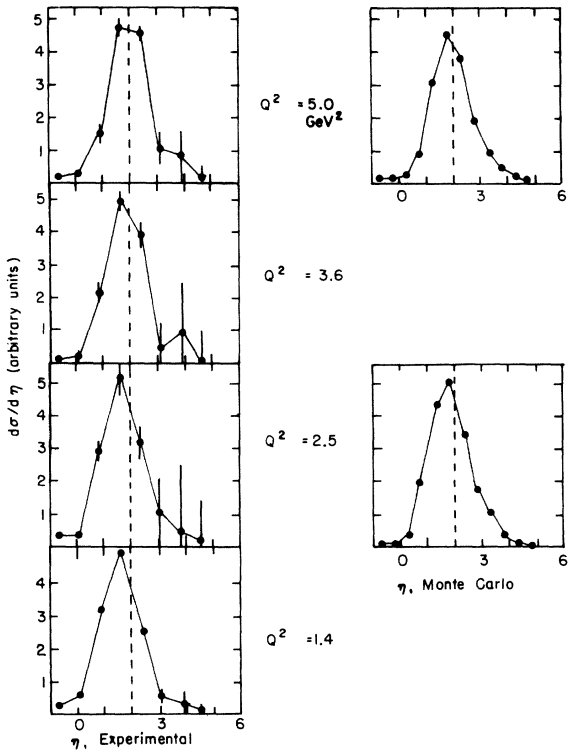

FIG. 18. Inclusive distributions of ep-electroproduced hadrons in pseudorapidity, $\eta = -\ln\tan(\theta_{\rm lab}/2)$ at fixed $s = 7$ GeV^2, and several Q^2 values. The vertical scale is proportional to the virtual-photon-plus-proton differential cross section $d\sigma/d\eta$; $\theta_{\rm lab}$ is measured with respect to the virtual-photon direction. Experimental and simulated data are compared (see text).

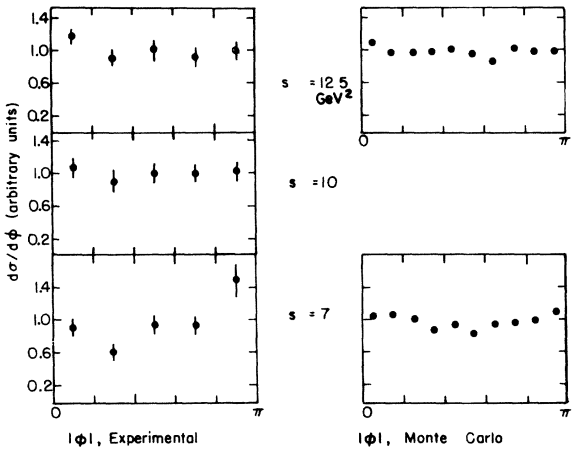

FIG. 19. Inclusive azimuthal distributions of ep-electroproduced hadrons about the virtual-photon direction, at fixed $Q^2 = 2.5$ GeV^2, and various s. The vertical scale is proportional to the virtual-photon-plus-proton differential cross section $d\sigma/d\phi$; the scattered electron is at $\phi = 0$. Experimental and simulated data are compared (see text).

VIC) are shown for comparison. One observes a broadening of the distributions as s increases at fixed Q^2 (Fig. 17). This is a kinematical effect related to the fact that the allowed rapidity range increases as $\ln s$. The same effect shows up in the Monte Carlo spectra. One can also see a slight shift of the centroid to higher η as Q^2 increases at fixed s (Fig. 18). This is also a kinematic effect, caused by the dependence on Q^2 of the relative velocity of the center-of-mass and laboratory frames. Again the same effect shows up in the Monte Carlo calculation. A simple extrapolation of low Q^2 data is therefore sufficient to explain the η distribution up to high values of Q^2. In particular, we do not see any evidence for increasing multiplicity in the photon fragmentation region.

D. Azimuthal distributions

The fitted $|\phi|$ distributions are plotted in Figs. 19 and 20. Although the Monte Carlo distributions show some evidence of the asymmetry in absorbing material around the target caused by the hydrogen supply tube, the asymmetry in the data, especially at low s, is significantly larger. The effect is rather independent of Q^2 and becomes

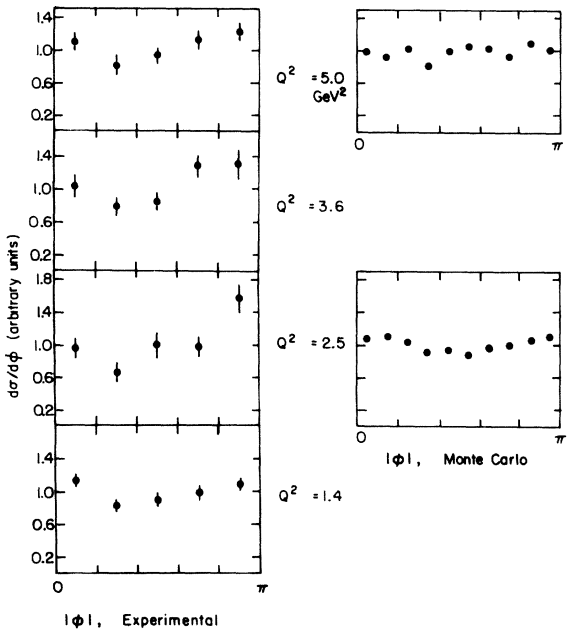

FIG. 20. Inclusive azimuthal distributions of ep-electroproduced hadrons about the virtual-photon direction, at fixed $s = 7$ GeV^2, and various Q^2. The vertical scale is proportional to the virtual-photon-plus-proton differential cross section $d\sigma/d\phi$; the scattered electron is at $\phi = 0$. Experimental and simulated data are compared (see text).

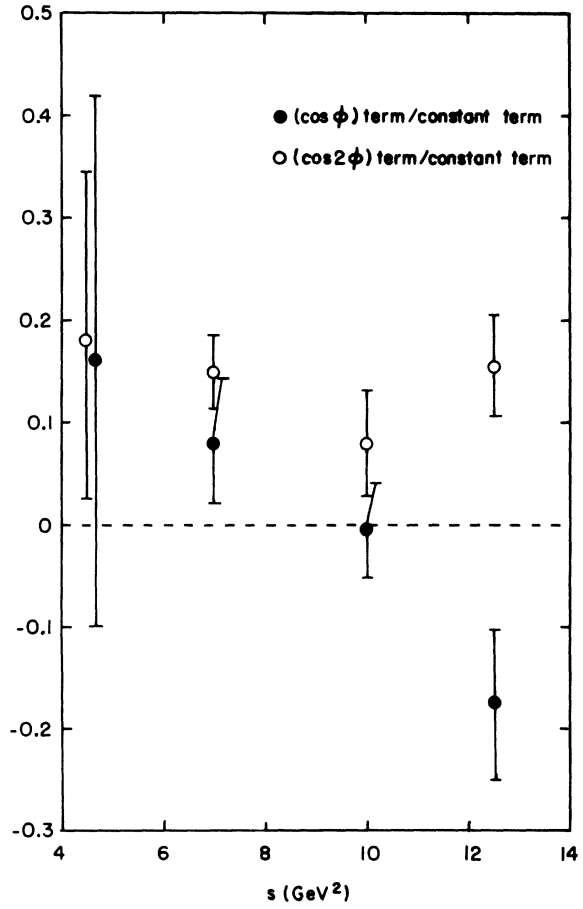

FIG. 21. s dependence at fixed $Q^2=2.5$ GeV^2 of the coefficients C_1/C_0 and C_2/C_0 in the expansion $C_0+C_1\cos\phi+C_2\cos2\phi$ of the inclusive azimuthal dependence in $e+p\rightarrow e+$hadrons.

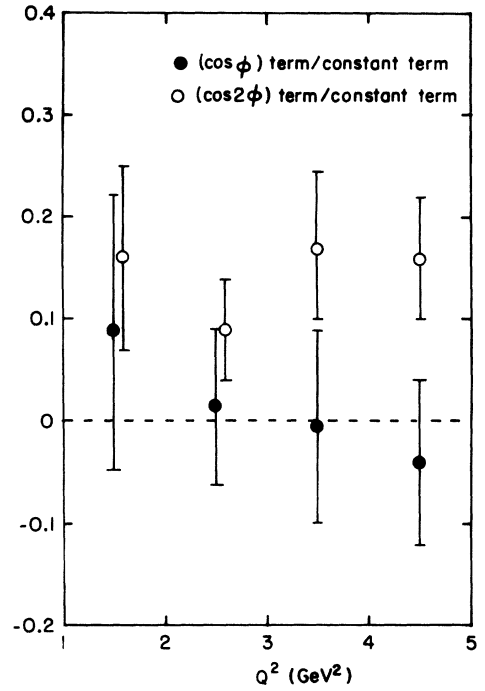

FIG. 22. Q^2 dependence at fixed $s=7$ GeV^2 of the coefficients C_1/C_0 and C_2/C_0 in the expansion $C_0+C_1\cos\phi+C_2\cos2\phi$ of the inclusive azimuthal dependence in $e+p\rightarrow e+$hadrons.

less pronounced as s increases.

To investigate the ϕ dependence further we have refitted the data contained in the three most populated η bins, avoiding the forward and backward angles, where any ϕ asymmetries must vanish. We have used a nonfactorized η and ϕ distribution of the form

$$C_0(\eta)+C_1(\eta)\cos\phi+C_2(\eta)\cos2\phi, \tag{16}$$

as required by the single-photon-exchange hypothesis.[39] The dependence on the virtual-photon polarization is averaged over our experimental ϵ range and absorbed into the C coefficients in (16). The results for C_1/C_0 and C_2/C_0 are shown in Figs. 21 and 22, averaged over η and s or Q^2. The coefficient C_1, arising from transverse-longitudinal interference,[39] is consistent with zero over the range of our data. C_2, the transverse polarization asymmetry, is slightly positive, giving C_2/C_0 about 15% typically.

A similar but more pronounced azimuthal asymmetry has been observed in photoproduction by transversely polarized photons.[28] There the effect shows up only for pions and with rather large forward momentum, and is ascribed to the decay of polarized ρ mesons. Previous electroproduction experiments[8,40] have found rather flat distributions.

Ravndal[41] has argued from the parton model that at high Q^2 and s there should be little or no ϕ asymmetry in the produced hadrons, and that C_1/C_0 and C_2/C_0 should decrease as $1/Q^2$. Since our observed asymmetry is actually not very large, and our Q^2 and s range not very high, we are not in serious disagreement with that prediction.

E. Deuterium angular distributions

The statistical accuracy of the data taken with the deuterium target is not sufficient to enable us to combine them with the hydrogen data and unfold meaningful η and ϕ distributions for *en* scattering. We have, however, compared the raw experimental distributions of counts over the scintillator array for the *ep* and *ed* runs and have noted no statistically significant differences. This suggests that angular distributions in *en*

electroproduction are similar to those measured in *ep* scattering. It also confirms that very few spectator protons were detected. They would have been isotropic in the lab, in contrast to the forward-peaked distribution of electroproduced secondaries.

XI. CONCLUSIONS

We have observed for virtual-photon-nucleon collisions in the range $1.4 \leq Q^2 \leq 8$ GeV^2 and $3 \leq s \leq 14$ GeV^2 that mean multiplicity, relative prong cross sections, rapidity distributions, and azimuthal distributions are all independent of Q^2 at fixed s. Above the resonance region the s dependence of the average charged hadron multiplicity is the same whether the colliding particles are real or virtual photons, baryons or mesons, positive or negative, or neutral, and whether it is the total multiplicity or the associated multiplicity. This strongly suggests that such global features of the final states are not determined from the dynamics of the collision, point-like or otherwise, but merely from the thermodynamics of hadronic matter and its energy of excitation.

---

*Work supported by National Science Foundation.

†On leave at DESY, 2 Hamburg 52, Germany.

‡Present address: Laboratory for Nuclear Science, MIT, Cambridge, Massachusetts 02139.

§Present address: Physics Department, University of Wisconsin, Madison, Wisconsin 53706.

[1]Theory and experiment for inclusive hadron reactions have been reviewed by W. R. Frazer *et al.*, Rev. Mod. Phys. 44, 284 (1972).

[2]The prototype of thermodynamic models is that by E. Fermi, Prog. Theor. Phys. 5, 570 (1950). A more recent version has been applied to electroproduction by P. Carruthers and M. Duong-van, Phys. Lett. 44B, 507 (1973).

[3]T. T. Chou and C. N. Yang, Phys. Rev. D 4, 2005 (1971).

[4]J. D. Bjorken, in *Proceedings of the 1971 Symposium on Electron and Photon Interactions at High Energies*, edited by N. B. Mistry (Laboratory of Nuclear Studies, Cornell University, Ithaca, N. Y., 1972).

[5]R. N. Cahn, J. W. Cleymans, and E. W. Colglazier, Pyys. Lett. 43B, 323 (1973).

[6]S. D. Drell, D. J. Levy, and T.-M. Yan, Phys. Rev. Lett. 22, 744 (1969).

[7]S.-S. Shei and D. M. Tow, Phys. Rev. Lett. 26, 470 (1971); S. Nussinov and A. Rangwala, Phys. Rev. D 5, 220 (1972).

[8]V. Eckardt *et al.*, contribution cited by F. W. Brasse, in *Proceedings of the Sixth International Symposium on Electron and Photon Interactions at High Energy, Bonn, Germany, 1973*, edited by H. Rollnik and W. Pfeil (North-Holland, Amsterdam, 1974), p. 251. See also V. Eckardt *et al.*, Nucl. Phys. B55, 45 (1973).

[9]J. Ballam *et al.*, contribution cited by F. W. Brasse (see Ref. 8).

[10]The multiplicity results of this experiment have been published previously: P. H. Garbincius *et al.*, Phys. Rev. Lett. 32, 328 (1974) (proton data); A. J. Sadoff *et al.*, *ibid.* 32, 955 (1974) (neutron data).

[11]J. W. DeWire, Cornell Report No. CLNS-104, 1970 (unpublished).

[12]We are indebted to D. Hartill for valuable assistance in the use of the proportional chamber system.

[13]We are grateful to F. M. Pipkin and the Harvard visiting group at the Cornell Synchrotron for the loan of the shower telescope and scintillation counter hodoscope.

[14]We are indebted to K. I. Greisen for the loan of the 68 photomultipliers.

[15]Radiation during scattering was calculated using the equivalent radiator approximation: L. W. Mo and Y.-S. Tsai, Rev. Mod. Phys. 41, 205 (1969).

[16]O. Pène and A. Krzywicki, Nucl. Phys. B12, 45 (1969). See also the discussion of the method of F. James in E. Byckling and K. Kajantie, *Particle Kinematics* (Wiley, New York, 1973).

[17]For more detail see P. H. Garbincius, Ph.D. thesis, Cornell University, 1974 (unpublished).

[18]E. Lazarus *et al.*, Phys. Rev. Lett. 29, 743 (1972).

[19]E. Lazarus *et al.*, Phys. Rev. Lett. 29, 1409 (1972).

[20]C. J. Bebek *et al.*, Phys. Rev. Lett. 32, 27 (1974). Similar data have been obtained by other groups at lower Q^2.

[21]C. Berger *et al.*, Phys. Lett. 47B, 377 (1973).

[22]J. M. Bailey *et al.*, contribution cited by F. W. Brasse (see Ref. 8); also D. L. Hartill (private communication).

[23]L. Ahrens *et al.*, Phys. Rev. D 9, 1894 (1974).

[24]C. J. Bebek *et al.*, Phys. Rev. Lett. 30, 624 (1973). Similar data have been obtained by other groups at lower Q^2.

[25]A. Bodek *et al.*, Phys. Rev. Lett. 30, 1087 (1973).

[26]We have used the Reid soft-core S- and D-state deuteron wave function: R. V. Reid, Ann. Phys. (N.Y.) 50, 411 (1968).

[27]We are indebted to H. A. Bethe and K. Gottfried for useful discussions on estimating the final-state interactions.

[28]K. C. Moffeit *et al.*, Phys. Rev. D 5, 1603 (1972).

[29]C. N. Brown *et al.*, Phys. Rev. D 8, 92 (1973); C. Driver *et al.*, Nucl. Phys. B30, 245 (1971); A. Sofair *et al.*, *ibid.* B42, 369 (1972).

[30]For definitions and predictions of scaling in ω, ω', and ω_w see J. D. Bjorken, Phys. Rev. 179, 1547 (1969); E. D. Bloom and F. J. Gilman, Phys. Rev. D 4, 2901 (1971); V. Rittenberg and H. R. Rubinstein, Phys. Lett. 35B, 50 (1971).

[31]See, for example, the review of M. Jacob, in *Proceedings of the XVI International Conference on High*

Energy Physics, Chicago-Batavia, Ill., 1972, edited by J. D. Jackson and A. Roberts (NAL, Batavia, Ill., 1972), Vol. 3, p. 373.

[32]We have set $C_{e\bar{e}}$ equal to the average value of $\bar{n}/\ln(E_{\text{tot}}^2)$, using the data of G. Tarnopolsky *et al.*, Phys. Rev. Lett. 32, 432 (1974). Similar charged multiplicity data were reported for the SLAC colliding beam experiment by B. Richter at the Chicago meeting of the American Physical Society, 1974 (unpublished). For a list of references on the Frascati experiments at $s \approx 8$ GeV^2, see K. Strauch, in *Proceedings of the Sixth International Symposium on Electron and Photon Interactions at High Energies, Bonn, Germany, 1973,* edited by H. Rollnik and W. Pfeil (North-Holland, Amsterdam, 1974), p. 1.

[33]Z. Koba, H. B. Nielsen, and P. Olesen, Nucl. Phys. B40, 317 (1972).

[34]H. Bøggild *et al.*, Copenhagen report (unpublished).

[35]A. Ramanauskas *et al.*, Phys. Rev. Lett. 31, 1371 (1973).

[36]G. Alexander *et al.*, Phys. Rev. D 8, 712 (1973).

[37]O. Czyżewski and K. Rybicki, Nucl. Phys. B47, 633 (1972).

[38]T. Ferbel *et al.*, Phys. Rev. 137, B1250 (1965); 173, 1307 (1968). In obtaining $\bar{n}$ from the prong cross sections the elastic scatters were excluded.

[39]C. W. Akerlof *et al.*, Phys. Rev. 163, 1482 (1967), Appendix I.

[40]J. T. Dakin *et al.*, Phys. Rev. Lett. 29, 746 (1972).

[41]F. Ravndal, Phys. Lett. 43B, 301 (1973).

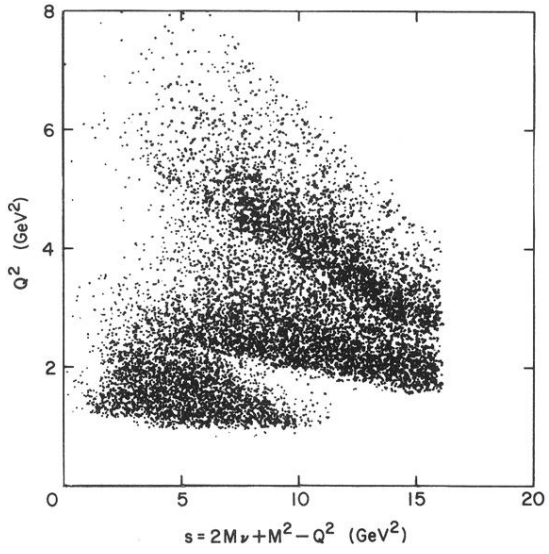

FIG. 3. Distribution of events in Q^2 and s for part of the hydrogen-target data.